Published in final edited form as:
Nature. 2014 May 29; 509(7502): 641–644. doi:10.1038/nature13232.

Dichloroacetate prevents restenosis in preclinical animal models of vessel injury

Tobias Deuse[1,2,3], **Xiaoqin Hua**[1,2], **Dong Wang**[1,2], **Lars Maegdefessel**[4], **Joerg Heeren**[5], **Ludger Scheja**[5], **Juan P. Bolaños**[6], **Aleksandar Rakovic**[7], **Joshua M. Spin**[8], **Mandy Stubbendorff**[1,2], **Fumiaki Ikeno**[8], **Florian Länger**[9], **Tanja Zeller**[2,10], **Leonie Schulte-Uentrop**[2,11], **Andrea Stoehr**[2,12], **Ryo Itagaki**[1,2], **Francois Haddad**[8], **Thomas Eschenhagen**[2,12], **Stefan Blankenberg**[2,10], **Rainer Kiefmann**[2,11], **Hermann Reichenspurner**[2,3], **Joachim Velden**[13], **Christine Klein**[7], **Alan Yeung**[8], **Robert C. Robbins**[14], **Philip S. Tsao**[8,15], and **Sonja Schrepfer**[1,2,3,14]

[1]TSI-laboratory, University Heart Center Hamburg, Martinistraße 52, 20246 Hamburg, Germany

[2]Cardiovascular Research Center Hamburg (CVRC) and DZHK (German Center for Cardiovascular Research), partner site Hamburg/Kiel/Luebeck, University Medical Center Hamburg-Eppendorf, Martinistraße 52, 20246 Hamburg, Germany

[3]Cardiovascular Surgery, University Heart Center Hamburg, Martinistraße 52, 20246 Hamburg, Germany

[4]Department of Medicine, Atherosclerosis Research Unit, Karolinska Institute, CMM L8:03, 17176 Stockholm, Sweden

[5]Department of Biochemistry and Molecular Cell Biology, University Medical Center Hamburg-Eppendorf, Martinistraße 52, 20246 Hamburg, Germany

[6]Institute of Functional Biology and Genomics, University of Salamanca-CSIC, Zacarias Gonzalez 2, 37007 Salamanca, Spain

[7]Institute of Neurogenetics, University of Lübeck, Maria-Goeppert-Straße 1, 23562 Lübeck, Germany

Correspondence and requests for materials should be addressed to S.S. (schrepfer@stanford.edu).

Online Content Any additional Methods, Extended Data display items and Source Data are available in the online version of the paper; references unique to these sections appear only in the online paper.

Supplementary Information is available in the online version of the paper.

Author Contributions T.D. designed the studies, performed surgical procedures, analysed the data and wrote the manuscript. X.H. and D.W. performed confocal immunofluorescence, immunohistochemistry, TMRM assays *in vivo* and *in vitro*, endothelial cell assays, the histopathological studies, analysed data and edited the manuscript. L.M. participated in designing experiments, analysed data, edited the manuscript and secured funding. J.H., L.S., J.P.B., A.R., J.M.S. and C.K. participated in designing experiments, analysed data and edited the manuscript. M.S. performed surgical procedures in rats, contributed to molecular biology experiments and flow cytometry. F.I. and A.Y. contributed to the swine coronary artery procedures and edited the manuscript. F.L. contributed to human coronary artery pathohistology data. T.Z. performed organ chamber experiments. L.S.-U. and R.K. contributed to the rabbit experiments. A.S. performed PCR experiments and analysed data. R.I. performed histology and immunological experiments. F.H. edited the manuscript. T.E., S.B. and H.R. edited the manuscript. J.V. performed histologic analyses. R.C.R. contributed to the study design and edited the manuscript. P.S.T. designed experiments, analysed data and edited the manuscript. S.S. designed the studies, performed surgical procedures in rats and rabbits, ran molecular biology experiments *in vitro* and *in vivo*, edited the manuscript and secured the funding.

The authors declare no competing financial interests.

[8]Cardiovascular Medicine and Stanford Cardiovascular Institute, Stanford University, 300 Pasteur Drive, Stanford, California 94305, USA

[9]Institute of Pathology, Hannover Medical School, Carl-Neuberg-Straße 1, 30625 Hannover, Germany

[10]Department of General and Interventional Cardiology, University Heart Center Hamburg, Martinistraße 52, 20246 Hamburg, Germany

[11]Department of Anaesthesiology, University Medical Center Hamburg-Eppendorf, Martinistraße 52, 20246 Hamburg, Germany

[12]Institute of Experimental Pharmacology and Toxicology, University Medical Center Hamburg-Eppendorf, Martinistraße 52, 20246 Hamburg, Germany

[13]Department of Nephropathology, Institute of Pathology, University Hospital Erlangen, Krankenhausstraße 8-10, 91054 Erlangen, Germany

[14]Department of Cardiothoracic Surgery and Stanford Cardiovascular Institute, Stanford University, 300 Pasteur Drive, Stanford, California 94305, USA

[15]Veterans Affairs Palo Alto Health Care System, 3801 Miranda Avenue, Palo Alto, California 94304, USA

Abstract

Despite the introduction of antiproliferative drug-eluting stents, coronary heart disease remains the leading cause of death in the United States[1]. In-stent restenosis and bypass graft failure are characterized by excessive smooth muscle cell (SMC) proliferation[2,3] and concomitant myointima formation with luminal obliteration. Here we show that during the development of myointimal hyperplasia in human arteries, SMCs show hyperpolarization of their mitochondrial membrane potential ($\Delta\Psi m$) and acquire a temporary state with a high proliferative rate and resistance to apoptosis. Pyruvate dehydrogenase kinase isoform 2 (PDK2) was identified as a key regulatory protein, and its activation proved necessary for relevant myointima formation. Pharmacologic PDK2 blockade with dichloroacetate or lentiviral PDK2 knockdown prevented $\Delta\Psi m$ hyperpolarization, facilitated apoptosis and reduced myointima formation in injured human mammary and coronary arteries, rat aortas, rabbit iliac arteries and swine (pig) coronary arteries. In contrast to several commonly used antiproliferative drugs, dichloroacetate did not prevent vessel re-endothelialization. Targeting myointimal $\Delta\Psi m$ and alleviating apoptosis resistance is a novel strategy for the prevention of proliferative vascular diseases.

Balloon injury of Lewis rat aortas triggered an inflammatory response and caused leukocyte infiltration in the SMC-rich media after 48 h, consisting mainly of CD68-positive ($CD68^+$) macrophages and some myeloperoxidase-positive (MPO^+) neutrophils;$CD3^+$ lymphocytes were not observed (Extended Data Fig. 1a–c). Compared to healthy, non-injured aortas, we observed increased phosphorylation of AKT (pAKT), and ERK1, ERK2 (pERK1/2) and $\Delta\Psi m$ hyperpolarization in media cells of injured vessels (Extended Data Fig. 1d, e). A myointima subsequently developed luminal to the internal elastic lamina, which caused progressive luminal obliteration over 28 days (Extended Data Fig. 1f, g). This process was

accompanied by leukocyte infiltration and inflammatory cytokine release, which was strong after 7 days and markedly reduced at 28 days (Extended Data Fig. 1h, i).

A humanized model was subsequently developed to study myointima formation longitudinally in human arteries. Balloon-injured human internal mammary arteries (HMAs) were implanted into the abdominal aortic position of T-cell-deficient Rowett nude (RNU) rats (Supplementary Video 1). Myointimal hyperplasia rapidly developed over 4 weeks (Fig. 1a) causing progressive luminal obliteration (Fig. 1c). By histopathology (Fig. 1b) and confocal immunofluorescence (Extended Data Fig. 2a, b), the myointima in the HMA model after 28 days or later closely resembled lesions of diseased human coronary arteries retrieved from autopsy samples. Using human leukocyte antigen class I (HLA I) and rat MHC I antibodies, the human origin of the SMCs within the myointima was confirmed (Extended Data Fig. 2c). Only the mechanical vessel injury was causally related to myointima formation and no relevant xenoantigen-triggered immune activation was observed (Extended Data Fig. 3a, b). Similar to the immunocompetent Lewis rat aortic injury model, we observed accumulation of $CD68^+$ macrophages and MPO^+ neutrophils in HMA vessels after 7 days, which was markedly attenuated by day 28 (Extended Data Fig. 3c). Immune cell infiltration was again accompanied by the elevation of inflammatory cytokines (Extended Data Fig. 3d).

Analysis of cell growth dynamics in HMAs showed a transient but strong increase in proliferative activity within the myointima between 7 and 21 days after injury, accompanied by a persistently low rate of apoptosis (Fig. 1d, e). Proliferation and apoptosis leveled off after 28 days when there was also no further progression of myointimal disease (Fig. 1c, e). Only during the time period of highly positive net proliferation did myointimal cells demonstrate $\Delta\Psi m$ hyperpolarization (Fig. 1f). Within the myointima, cells in the luminal region showed higher proliferative activities and higher $\Delta\Psi m$ than cells closer to the media (Extended Data Fig. 3e).

Platelet-derived growth factor (PDGF) was suspected to be the major driving factor promoting myointimal hyperplasia as it was temporarily increased in injured HMA vessels and PDGF receptor blockade prevented the development of relevant disease (Extended Data Fig. 3f, g). Human vascular SMCs were isolated from fresh HMAs and characterized (Extended Data Fig. 4a, b). PDGF was then shown to induce $\Delta\Psi m$ hyperpolarization in cultured SMCs (Extended Data Fig. 4c), similar to the $\Delta\Psi m$ hyperpolarization previous observed in injured HMAs (Fig. 1f). Thus, mitochondrial $\Delta\Psi m$ hyperpolarization in myointimal SMCs and cultured SMCs coincided with the availability of PDGF. PDGF also caused a phenotype switch in SMCs from a contractile to a dedifferentiated state (Extended Data Fig. 4d).

Mitochondria have been shown to regulate apoptosis via their mitochondrial apoptotic pathway[4]. This involves mitochondrial permeability transition and the release of toxic components such as cytochrome C and caspases[5]. In this context, $\Delta\Psi m$ has an important role in the control of the mitochondrial permeability transition pore, as $\Delta\Psi m$ hyperpolarization has been suspected to impede pore opening[6,7]. Dichloroacetate (DCA), a rapid-acting small molecule targeting mitochondrial PDKs, has previously been

demonstrated to reduce ΔΨm in A549 cells[8]. As elevated ΔΨm and suppressed apoptosis have been observed after injury in our HMA model, we reasoned that DCA would prevent post-injury ΔΨm hyperpolarization, facilitate apoptosis and reduce myointimal growth.

DCA effectively prevented ΔΨm hyperpolarization in PDGF-treated SMCs isolated from either healthy or atherosclerotic vessels (Extended Data Fig. 5a, b). Previously, mitochondrial cytochrome C release and apoptosis induction were shown to be suppressed by hyperpolarized ΔΨm[7,9]. Consistent with this observation, PDGF reduced staurosporine-induced mitochondrial cytochrome C leakage (Extended Data Fig. 5c, d) and rendered SMCs resistant to apoptosis (Extended Data Fig. 5e). DCA both increased cytochrome C release and restored the ability to enter apoptosis (Extended Data Fig. 5c–e).

In vivo, oral DCA did not affect leukocyte infiltration in the media of balloon-injured aortas in immunocompetent Lewis rats, but effectively lowered ΔΨm in the media at 48 h (Extended Data Fig. 6a–d). The accumulation of $CD68^+$ macrophages and MPO^+ neutrophils in the developing myointima was also not affected by DCA (Extended Data Fig. 6e). However, at 7 days, DCA markedly reduced myointimal ΔΨm and permitted apoptosis (Extended Data Fig. 6f, h). At 28 days, ΔΨm in the developed control myointima had already lowered and DCA showed little effect (Extended Data Fig. 6g). Also, proliferation and apoptosis were low at that time point (Extended Data Fig. 6i).

The potential vasculoprotective effect of DCA was then tested in the HMA and human coronary artery (HCA) models (Fig. 2a–d). For the latter, HCAs with minor pre-existing disease, which underwent the same balloon injury and implantation procedure as described for HMA, were used to better reflect the coronary pathophysiology. Oral DCA administration strongly reduced the development of myointima and luminal narrowing in both HMAs (Fig. 2a) and HCAs (Fig. 2d). Similar to untreated HMA controls, the proliferative response to injury in DCA-treated vessels was strongest within the first 14 days and weakened thereafter (Fig. 2b). However, the apoptotic activity was also enhanced and mirrored the proliferative activity at each time point, resulting in a much lower net proliferation. In accordance with the *in vitro* data, we observed significantly lower ΔΨm in the 21-day HMA specimens of the DCA group (Fig. 2c). To exclude the possibility that ischaemia-reperfusion injury or xenogeneic immune interactions might have affected our results, DCA was tested further in the rat aortic (Fig. 2e) and the rabbit iliac artery balloon injury models (Fig. 2f). Again, myointima formation after 28 days was remarkably reduced by DCA in both models. Interestingly, DCA neither demonstrated anti-migratory effects on endothelial cells *in vitro* nor inhibited vessel re-endothelialization *in vivo* (Extended Data Fig. 7 and Supplementary Video 2).

PDKs are the only known targets of DCA and PDKs exclusively phosphorylate and thus inactivate pyruvate dehydrogenase (PDH). It was therefore suspected that PDK knockdown would generate similar biological effects as PDK inhibition by DCA. Although SMCs express PDK1, PDK2 and PDK3 (Extended Data Fig. 8a), PDK2 has the highest affinity to DCA[10] and is likely to mediate the vast majority of the DCA effect. Therefore, PDK2-knockdown SMCs were generated using *PDK2* lentiviral short hairpin RNA (shRNA) (Extended Data Fig. 8b, c) to verify the mechanistic involvement of PDK2 in the DCA

effect. Indeed PDK2-knockdown SMCs maintained steady low ΔΨm (Extended Data Fig. 9a) under control conditions and with PDGF stimulation. Also, PDK2-knockdown SMCs maintained increased cytochrome C release and elevated apoptotic rates even during PDGF incubation (Extended Data Fig. 9b–d). In addition, DCA lost its ability to affect ΔΨm in PDK2-knockdown SMCs (Extended Data Fig. 9a). As expected, when PDH (the primary inhibitory target of PDK2) was knocked down (Extended Data Fig. 9e) instead of PDK2, the opposite effect was observed: ΔΨm was permanently elevated, even under control conditions (Extended Data Fig. 9f). DCA again lost its ability to depolarize ΔΨm, indicating that the DCA effect on ΔΨm depended on both PDK2 and PDH.

To assess whether arteries with *ex vivo* PDK2 knockdown would develop similarly reduced myointima as arteries under DCA treatment, PDK2 knockdown was induced in HMAs and HCAs before implantation (Extended Data Fig. 8d–f). Comparable to the DCA group, PDK2-knockdown HMAs showed low net proliferation throughout the 28-day study period (Fig. 3a). ΔΨm hyperpolarization was also effectively prevented and the low ΔΨm of PDK2 knockdown HMAs at day 21 (Fig. 3b) closely resembled the ΔΨm values of DCA-treated HMAs (Fig. 2c). Reduced luminal obliteration was observed in both PDK2-knockdown HMAs (Fig. 3c) and HCAs (Fig. 3d) at day 28.

DCA was ultimately evaluated in a translationally relevant swine model of coronary artery restenosis. Yorkshire swine underwent standardized coronary artery balloon injury under fluoroscopic guidance. After 28 days, DCA-treated animals showed significantly reduced luminal obliteration, proliferation area, and max. proliferation thickness (Fig. 4a–d). In summary, DCA reduced myointima formation in five different preclinical *in vivo* models.

Upon PDGF stimulation of cultured SMCs, we observed an activation of the downstream PI(3)K (phosphatidylinositol-3-OHkinase) and MEK (MAPK kinase) pathways with AKT phosphorylation, ERK1 and ERK2 phosphorylation, hexokinase 2 (HK2) upregulation, and increased HK2–mitochondrial association (Extended Data Fig. 10a–d). HK2 has previously been shown to have a binding site close to VDAC (voltage-dependent anion-selective channel), the most abundant protein of the outer mitochondrial membrane, and HK2 binding was reported to reduce channel conductance[11,12]. Consistent with this previous work, we show that HK2–mitochondrial association coincides with ΔΨm hyperpolarization and apoptosis resistance in our study. Furthermore, displacement of HK2 from its mitochondrial VDAC binding site both reduced ΔΨm and restored the susceptibility to apoptosis (Extended Data Fig. 10e). VDAC closure using the inhibitor DIDS also increased SMC ΔΨm and reduced apoptosis (Extended Data Fig. 10f), further supporting the direct mechanistic involvement of VDAC in the regulation of both ΔΨm and apoptosis.

DCA and PDK2 knockdown diminished HK2 elevation (Extended Data Fig. 10b) and HK2–mitochondrial association (Extended Data Fig. 10c, d), and maintained low ΔΨm despite PDGF (Extended Data Fig. 10g). Notably, it was confirmed that the depolarizing effects of DCA and PDK2 knockdown on ΔΨm were ultimately mediated through VDAC, because inhibition of VDAC opening by DIDS was found to neutralize these effects (Extended Data Fig. 10g). However, the mechanistic link between PDK2 inhibition and the decrease in HK2-VDAC binding and reversal of ΔΨm hyperpolarization remains elusive.

In healthy vessels, proliferation and apoptosis are very low and balanced[13]. Vessel injury disrupts this homeostasis and triggers an inflammatory state[14–16], which induces temporary ΔΨm hyperpolarization in SMCs and drives myointima formation. As shown here, PDK2 repression counteracts temporarily acquired apoptosis resistance and may be a well-tolerated strategy for the prevention of restenosis without interfering with re-endothelialization.

METHODS

Animal models

HMAs were obtained during routine coronary artery bypass surgery and HCAs without stenotic disease or calcifications were obtained from patients <50 years of age undergoing heart transplantation for dilated cardiomyopathy. The use of leftover arteries from the operating room for research was approved by the Institutional Review Board (IRB) and patients gave their written informed consent. Human myointimal hyperplasia was induced in HMAs and HCAs by balloon injury using a 2-French Fogarty catheter and the human arteries were implanted into the abdominal aortic position of male athymic RNU rats (8 weeks old; Crl:NIH-*Foxn1*^{rnu}; Charles River, Sulzfeld, Germany). Male Lewis rats (8 weeks old) and male New Zealand rabbits (12 weeks old, Charles River) underwent balloon injury of their abdominal aortas or their iliac arteries, respectively, using Fogarty catheters. Rats and rabbits in the DCA groups were treated with DCA (0.75 g l^{-1} in drinking water, Sigma, Munich, Germany). The PDGF-R blocker imatinib (50 mg kg^{-1} day^{-1}, oral) was administered in one experiment. Animals were excluded if they died prematurely or became sick, as diagnosed by a veterinarian. Vessels in the PDK2-knockdown HMA or HCA groups underwent *ex vivo* PDK2 knockdown on the day before implantation. Rat and rabbit studies were approved by the Hamburg Amt für Gesundheit und Verbraucherschutz. Naturally diseased human coronary artery samples were recovered at autopsy from patients with myointimal hyperplasia at 54 to 63 years of age.

Swine study

Swine experiments were performed according to the protocol approved by the Stanford University Administrative Panel on Laboratory Animal Care (APLAC). A total of 10 female juvenile Yorkshire swine (40–50 kg, 12–14 weeks old) were used for this study. Swine were pretreated with aspirin (650 mg) and nifedipine (30 mg) orally at least 12 h before the injury procedure. The animals were sedated with telazol (6 mg kg^{-1}, intramuscular), followed by inhalant mask induction (isoflurane 4–5%). Following intubation, anaesthesia was maintained with 1–3% isoflurane in a mixture of oxygen and air. Animals were placed in the supine position and continuous electrocardiography and haemodynamic monitoring were performed throughout all procedures.

Vascular access was obtained using a standard 6-French vascular sheath placed in the right or left carotid and/or femoral arteries, as necessary. All animals received pre-procedural heparin (300 IU kg^{-1}, intra-arterial) and an activated clotting time was maintained at >300 s.

After advancing a 6-French guiding catheter through the aorta into the coronary ostia, an intracoronary injection of 0.2 mg nitroglycerin was administered and baseline coronary

angiography was performed to identify the desirable location for the lesion based on coronary artery size and anatomy. A 0.014-inch percutaneous transluminal coronary angioplasty guidewire was advanced through the guiding catheter into the coronary artery. A bare metal coronary stent was implanted distal to the target lesion site to achieve a 1.05–1.15:1 stent–artery ratio as a marker. Balloon injury was induced at 10–20 mm proximal from the marker stent to achieve a 1.3–1.35:1 balloon–artery overstretch. The balloon was inflated for 30 s twice with a 30-s interval. Three coronary arteries, the left anterior descending artery, the circumflex artery and the right coronary artery were used in all animals. Subsequently, coronary artery patency was confirmed by coronary artery angiography. The animals were weaned from mechanical ventilation and allowed to recover in their normal housing at the animal care facility. Swine in the treatment group received DCA at 25 mg kg^{-1} three times a day. The animals were monitored daily until the time of coronary artery retrieval at 4 weeks after euthanasia. A total of 45 sections were analysed per group (three sections per vessel, three coronary arteries per pig, five pigs per group).

Histology and immunohistochemistry

Vessels were stained with Masson's trichrome for quantification of the luminal obliteration, which was defined as the percentage of the cross-sectional area within the internal elastic lamina taken up by the myointima. The overview vessel images in the figures show cropped vessels without surrounding tissue. RECA-1 (HIS52, Serotec, Raleigh, North Carolina) was used to stain endothelium. CD3 (SP7), CD68 (ED1, Abcam) and MPO (no.475915, Calbiochem) staining characterized leukocyte infiltration.

Cytokine antibody array

Injured rat aortas or HMAs were recovered and homogenized in cell lysing buffer (including proteinase inhibitor) using the Qiagen Tissue Lyser. Tissue lysate (400 μg) was diluted in 1 ml assay buffer and membranes were incubated for 2 h at 20–25 °C followed by antibody incubation according to the protocol. Cytokine antibody arrays for PDGF, IFNγ, MCP-1, MIP-3α, and IL-1β (Raybiotech, Norcross, Georgia, USA) were performed according to the manufacturer's protocol. The membranes were digitized using bioluminescence imaging and quantified using NIH ImageJ. Cytokine concentration is expressed in arbitrary units (AU).

Cell culture

Human vascular SMCs were freshly isolated from HMA or atherosclerotic coronary arteries using papain (1 mg ml^{-1}), dithiothreitol (0.5 mg ml^{-1}), collagenase (0.6 mg ml^{-1}) and bovine serum albumin (0.6 mg ml^{-1}, Sigma). SMCs were used for experiments when they were 70–80% confluent. SMCs were incubated with PDGF (50 ng ml^{-1}) for 48h and/or DCA (5 mM; DCA treatment was started 2 days before PDGF) if not indicated otherwise. The VDAC inhibitor diisothiocyanatostilbene-2,2′-disulfonic acid (DIDS, 0.5 mM for 24 h, Sigma) or HXK2VBD-cpm, a cell-permeable peptide analogue of the HK2-VDACbinding domain (100 μM, Advanced Peptide, Boston, MA), were used in some assays.

PDK2 knockdown

Lentiviral shRNA particles targeting *PDK2* (Santa Cruz, Santa Cruz, California) were used to knock down PDK2 *ex vivo* before HMA or HCA implantation, and *in vitro* using human SMCs. Lentiviral particles were a pool of three different shRNA plasmids: 5′-GATCCCCAAGTACATAGAGCACTTTTCAAGAGAAAGTGCTCTATGTACTTGGTTTTT-3′, 5′-GATCCGACCGATGCTGTCATCTATTTCAAGAGAATAGATGACAGCATCGGTCTTTTT-3′, 5′-GATCCCCAACTCTAAAGTGGAAGATTCAAGAGATCTTCCACTTTAGAGTTGGTTTTT-3′.

shRNA lentiviral particles containing an shRNA construct encoding a scrambled sequence served as control. Vessels were inflated with lentiviral-particle-containing medium (1×10^6 infectious units of virus per 200 μl); human SMCs were transduced at a multiplicity of infection of 50. Successfully transduced PDK2-knockdown SMCs were purified using puromycin.

PDH knockdown

SMCs (3×10^4) were transfected with 80 pmol of siRNA targeting *PDH* (Santa Cruz) in OptiMem (Gibco, Grand Island, New York) supplemented with transfection reagent (Santa Cruz) at 37 °C and 5% CO_2. *PDH* siRNA was a pool of three different siRNA duplexes: sense, 5′-CAGAUCAGCUGUAUAAACATT-3′; antisense, 5′-UGUUUAUACAGCUGAUCUGTT-3′; sense, 5′-GGAUUGCUCUAGCCUGUAATT-3′; antisense, 5′-UUACAGGCUAGAGCAAUCCTT-3′; sense, 5′-CUGUCACAUUCCUAUUUCUTT-3′, antisense: 5′-AGAAAUAGGAAUGUGACAGTT-3′.

After 6 h, the same volume of normal growth medium containing two times the normal serum and antibiotics concentration was added without removing the transfection mixture. After an additional 24 h, medium was replaced and cells were used for experiments 48 h after the transfection.

Elispot assays

For uni-directional Elispot assays, recipient splenocytes were isolated from fresh spleen 7 days after HMA or aortic transplantation and used as responder cells. Donor-specific non-transplanted HMA or aortic tissues were homogenized and single cells were mitomycin-inhibited and served as stimulator cells. Stimulator cells (10^5) were incubated with 10^6 recipient responder splenocytes for 24 h and IFNγ spot frequencies were automatically counted using an Elispot plate reader.

Endothelial-cell scratch assay

Endothelial cells (5×10^5 per well) were plated onto 6-well plates. When cells reached confluence, a scratch was made across the cell monolayer using a pipette tip (scratch width, 338 μm). Time to closure was monitored by living cell imaging (Improvision Spinning Disk;

Perkin Elmer, Waltham, Massachusetts, magnification × 100) for 24h. In addition, endothelial cells that migrated into the 340 μm × 338 μm scratch area were counted after 5 h.

Organ chamber experiments

Fresh vascular rings of rat aorta were cut into 4-mm segments and mounted in phosphate-buffer-filled organ chambers gassed with 95% oxygen and 5% carbon dioxide. After pre-constriction with prostaglandin F2α (15 μl 10^{-2} M in 25 ml buffer) to achieve 50–80% of the maximal KCl-induced tone, increasing concentrations of nitroglycerin (NTG, 10^{-9} M to $10^{-4.5}$ M) or acetylcholine (10^{-9} M to $10^{-5.5}$ M) were added for relaxation studies. Endothelium-dependent (acetylcholine) and -independent (NTG) vasodilator responses were assessed with denuded aortic rings serving as negative controls for endothelial function.

Immunoblot analysis

Proteins were separated on SDS–PAGE gels (Invitrogen, Carlsbad, California) and western blot analyses were conducted with specific antibodies to pAKT (D9E), pERK1/2 (#9101), GAPDH (14C10, Cell Signaling, Irvine, California), HK2 (1A7), PDH (9H9), PDK1 (C20), PDK2 (N20), PDK3 (N14), PDK4 (C16, Santa Cruz), SMA (ab5694), CV (ab110415), β-actin (ACTN05 (C4), Abcam), cytochrome C (6H2.B4, Calbiochem, Darmstadt, Germany), myocardin (355521, R+D Systems, Minneapolis, Minnesota), and SMemb (3H2, Yamasa, Tokyo, Japan). The membranes were digitized using bioluminescence imaging and quantified using NIH ImageJ. GAPDH or β-actin served as housekeeping control.

RNA quantification and PCR

Total RNA was isolated with a TRIzol-based (Invitrogen) RNA isolation protocol and RNA was quantified by NanoDrop (NanoDrop ND-1000, Peqlab, Erlangen, Germany). Samples required 260:280 ratios of >1.8 for inclusion. RNA was reverse-transcribed with the High Capacity cDNA Reverse Transcription Kit (Applied Biosystems, Foster City, California) according to them anufacturer's instructions. Quantitative determination of RNA was performed by real-time RT–PCR with POWER SYBR Green PCR Master Mix (Applied Biosystems) according to the manufacturer's instructions. Primers were used specific for every human sequence. Particularly, the primers used to amplify *PDK1-4* were: *PDK1* forward, 5′-AGTGCCTCTGGCTGGTTTTGG-3′ and reverse, 5′-CGTGGTTGGTGTTGTAATGCTTCC-3′; *PDK2* forward, 5′-GCAAGTTCTCCCCGTCCCCG-3′ and reverse, 5′-GGACATACCAGCTCTGCACCAG-3′; *PDK3* forward, 5′-CAGAGCTGCCCCTTTGGCTGG-3′ and reverse, 5′-TGGCGCCATGCGGACTTATT-3′ and *PDK4* forward, 5′-TGGTAGCAGTGGTCCAAGATGCC-3′ and reverse, 5′-CAACTGTTGCCCGCATTGCAT-3′. Absolute and relative RNA levels of *PDK1*, *PDK2*, *PDK3* and *PDK4* were determined to endogenous *GAPDH*. *c-KIT* RNA was amplified using primers forward, 5′-CACCGAAGGAGGCATTACAC-3′ and reverse, 5'-GGAATCCTGCTGCCACACA-3′. *SMA* RNA was amplified using primers forward, 5′-GCGTGGCTATTCCTTCGTTA-3′ and reverse, 5′-ATGAAGGATGGCTGGAACAG-3′. *SM22* RNA was amplified using primers forward, 5′-AACAGCCTGTACCCTGATGG-3′ and reverse, 5′-CGGTAGTGCCCATCATTCTT-3′. Experiments were performed on the

7900 HT Sequence Detection System (Applied Biosystems). The amount of RNA was estimated according to the comparative Ct method with the 2-ΔΔCt formula.

Immunofluorescence staining

Tissues were fixed with 4% paraformaldehyde, dehydrated and embedded in paraffin. After heat-induced antigen retrieval with Dako antigen retrieval solution (Dako, Glostrup, Denmark) in a steamer for 20 min, 3-μm paraffin sections were blocked with Image-iT FX signal enhancer (Invitrogen) for 30 min. Primary antibodies of following sources were used: SMA (ab5694), SM heavy chain (EPR5335), SM22 (ab10135), calponin (CALP), smoothelin (R4A, Abcam), Ki67 (SP6), CD3 (SP7), PDK1 (C20), PDK2 (N20), human leukocyte antigen I (HLAI, 3F10, Santa Cruz), myocardin (355521, R+D Systems), and rat major histocompatibility complex I (MHC I, B5) conjugated with FITC (BD Pharmingen). Except for MHC I staining, all other studies included incubation with a corresponding secondary antibody conjugated to Alexa Fluor 488, Alexa Fluor 555, or Alexa Fluor 647 (Invitrogen). Sections were incubated with antibodies for 1 h at 37 °C, followed by cell nucleus staining with DAPI for 10 min. Imaging was performed using a Nikon Eclipse TiE microscope (Nikon, Tokyo, Japan) equipped with the Perkin Elmer UltraVIEW VoX confocal imaging system (Perkin Elmer, Waltham, Massachusetts). Analysis was carried out with Volocity 6.1.1 (Perkin Elmer).

For co-localization of HK2 and mitochondria, confocal images stained for HK2 (1A7, Santa Cruz), MitoTracker (Invitrogen), and DAPI were obtained with the confocal Nikon Eclipse TiE microscope.

Flow cytometry by FACS

Primary antibodies used to characterize SMCs were SMA (ab5694), SM22 (ab10135), calponin (CALP), smoothelin (R4A, Abcam), and myocardin (355521, R+D Systems). Samples were measured on a FACSCalibur system (Becton Dickinson, Heidelberg, Germany) and analysed using FlowJo (Tree Star, Ashland, Oregon). In the histograms, the isotype controls are displayed in grey and the antigens of interest in green.

TMRM staining

To measure ΔΨm, freshly isolated tissues or cells were incubated with tetramethylrhodamine methyl ester perchlorate (TMRM, 10 nM; Invitrogen) and Hoechst 33342 (0.3 μM; Invitrogen) for 30 min at 37 °C. Subsequently, samples were washed to remove unbound dye and immediately imaged. *In vitro*, 5×10^4 SMCs were plated on confocal dishes and cells were stimulated according to their group-specific protocol. Vessels were freshly cut under the microscope into thin slices and were timely stained and analysed. Fluorescence signal was measured using a Nikon Eclipse TiE microscope equipped with Perkin Elmer UltraVIEW VoXconfocal imaging system. Analysis was carried out on Volocity 6.1.1. For analysis, mean TMRM-fluorescence intensity was calculated by dividing individual object fluorescence intensities by sizes (number of voxels) and is expressed in arbitrary fluorescence units (FU).

Cytochrome C staining

To measure cytochrome-C-related apoptosis, cells were stained for cytochrome C after staurosporine treatment (50 nM; Sigma) for 18 h. Cells were then fixed in 4% paraformaldehyde, permeabilized with Permeabilization Solution (Applied StemCell, Menlo Park, California), and blocked with Blocking Solution (Applied StemCell). After incubation with a mouse antibody against cytochrome C (6H2.B4, Calbiochem) for 16 h at 4 °C, a goat anti-mouse antibody conjugated with Alexa Flour 488 (Invitrogen) was used as the secondary antibody (1 h, 37 °C). Cell nuclei were counterstained with DAPI. Examination was carried out with a Nikon Eclipse TiE microscope equipped with Perkin Elmer UltraVIEW VoX confocal imaging system, followed by analysis with Volocity 6.1.1. For analysis, cells showing diffuse cytoplasmatic cytochrome C staining overlying the nucleus were counted and divided by the number of DAPI positive cells to obtain the percentage of cells with cytochrome C leakage.

TUNEL staining

SMCs were treated with staurosporine (50 nM; Sigma) for 18 h to induce apoptosis. ApopTag apoptosis detection kit (TUNEL; Merck Millipore, Darmstadt, Germany) was then used according to manufacturer's instructions to label apoptotic cells. Similarly, tissue sections, processed as described in "Immunofluorescence staining", underwent heat-induced antigen retrieval with Dako antigen retrieval solution (Dako) in a streamer for 20 min, followed by blocking with Image-iT FX signal enhancer (Invitrogen) for 30 min. Staining was performed according to manufacturer's instructions using the ApopTag apoptosis detection kit. Nuclei were counterstained with DAPI. The percentage of TUNEL-positive cells was calculated.

Statistics

Owing to the exploratory character of this study and the fact that an inhibitory effect of DCA on myointima formation has not been described yet, there were no data for an initial power analysis. Usually, five to seven animals were randomized to one group. All samples were number coded until the readout was finalized. The numbers were assigned before the experiment and determined the group, treatment and condition. The surgeons performing the procedures and the scientists performing the readouts were blinded. All values are expressed as mean ± s.d. or mean ± s.e.m. as indicated. Intergroup differences were appropriately assessed by either unpaired two-tailed Student's *t*-test or one-way analysis of variance (ANOVA) with Bonferroni's post-hoc test. If data were normalized to the control group, one-sample *t*-tests against 1.0 were used for study groups. * $P < 0.05$, ** $P < 0.01$.

Extended Data

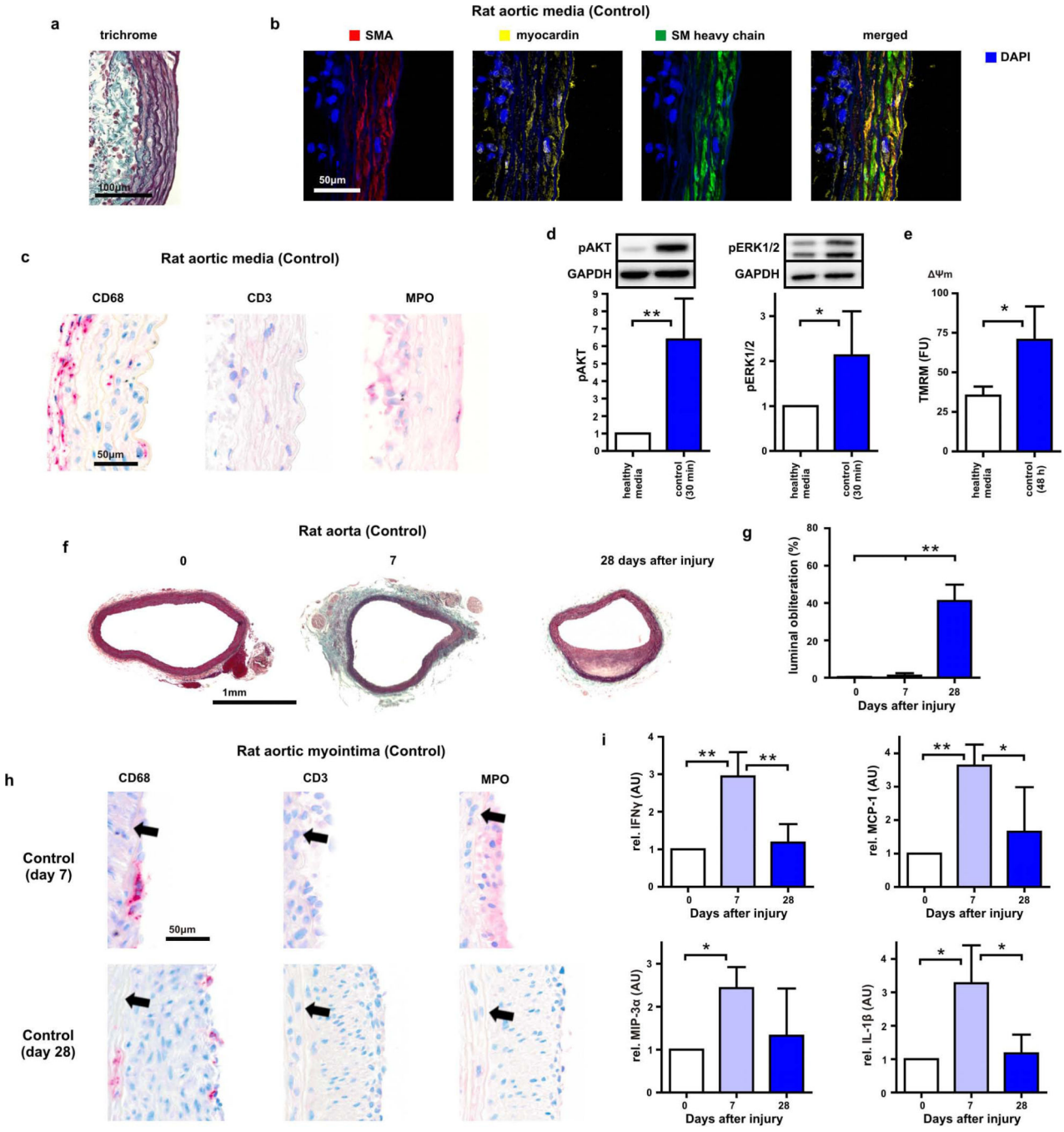

Extended Data Figure 1. Myointima formation in balloon-injured rat aortas

a, **b**, Forty-eight hours after mechanical injury, trichrome (**a**) and immunofluorescence for SMC-markers (**b**) identified abundant SMCs in the aortic media. **c**, The infiltrate at 48 h was composed of $CD68^+$ macrophages, some MPO^+ neutrophils, and no $CD3^+$ lymphocytes. **d**, Phosphorylation of AKT (pAKT), and ERK1 and ERK2 (pERK1/2), was markedly increased as early as 30 min after injury (mean ± s.d., *n* = 6 animals per group, control after

30 min normalized to healthy media, one-sample *t*-tests). **e**, Media cells of injured aortas showed ΔΨm hyperpolarization after 48 h (mean ± s.d., $n = 4$ animals (healthy media), 6 animals (control after 48 h), Student's *t*-test). **f, g**, A myointima developed over 28 days in injured rat aortas (**f**, trichrome) and caused luminal obliteration (**g**, mean ± s.d., $n = 5$ animals (day 0), 4 animals (day 7), 6 animals (day 28), ANOVA with Bonferroni's post-hoc test). **h**, Many infiltrating macrophages and very few neutrophils were observed in the myointima at 7 days. Leukocyte infiltration was sparse at 28 days; no lymphocytes were found (black arrows, internal elastic lamina). **i**, Tissue IFNγ, MCP-1, MIP-3α, and IL-1β levels were markedly increased at 7 days and were diminished after 28 days (mean ± s.d., $n = 3$ animals (day 0), 4 animals (day 7 and 28), days 7 and 28 normalized to day 0, one-sample *t*-test (day 0 versus day 7), Student's *t*-test (day 7 versus day 28)). $*P < 0.05$; $**P < 0.01$.

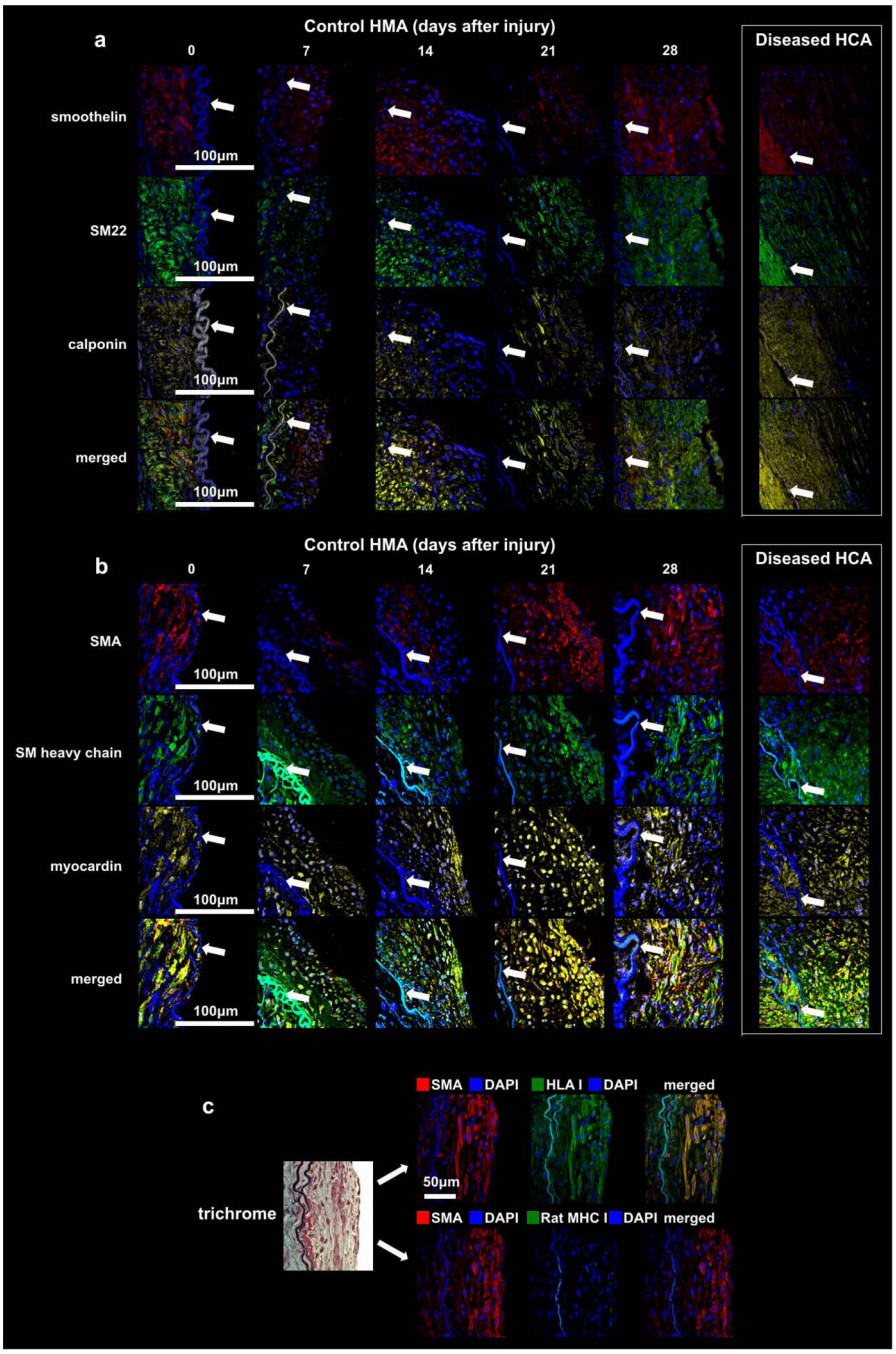

Extended Data Figure 2. Characterization of the human internal mammary artery model

a, **b**, Sections were co-stained for the SMC markers smoothelin, SM22, and calponin (**a**) or SMA, smooth muscle myosin (SM) heavy chain and myocardin (**b**). Co-localization could be observed in the merged pictures (white arrows, internal elastic lamina, pictures are representative of two replicates). Direct comparison between the HMA myointima on day 28 with the myointima in diseased human coronary artery (HCA) samples illustrated close similarities in immunofluorescence morphology. **c**, The human origin of myointimal cells in 21-day control HMAs was confirmed. Trichrome showed the development of a cell-rich

myointima with mild fibrosis. Specimens were stained for SMA, DAPI and human leukocyte antigen class I (HLA I, upper row) or rat major histocompatibility complex class I (rat MHC I, lower row). Cells expressing SMA (red) co-expressed HLA I (green), which resulted in a yellow staining in the merged picture. No co-expression of SMA and rat MHC I was observed.

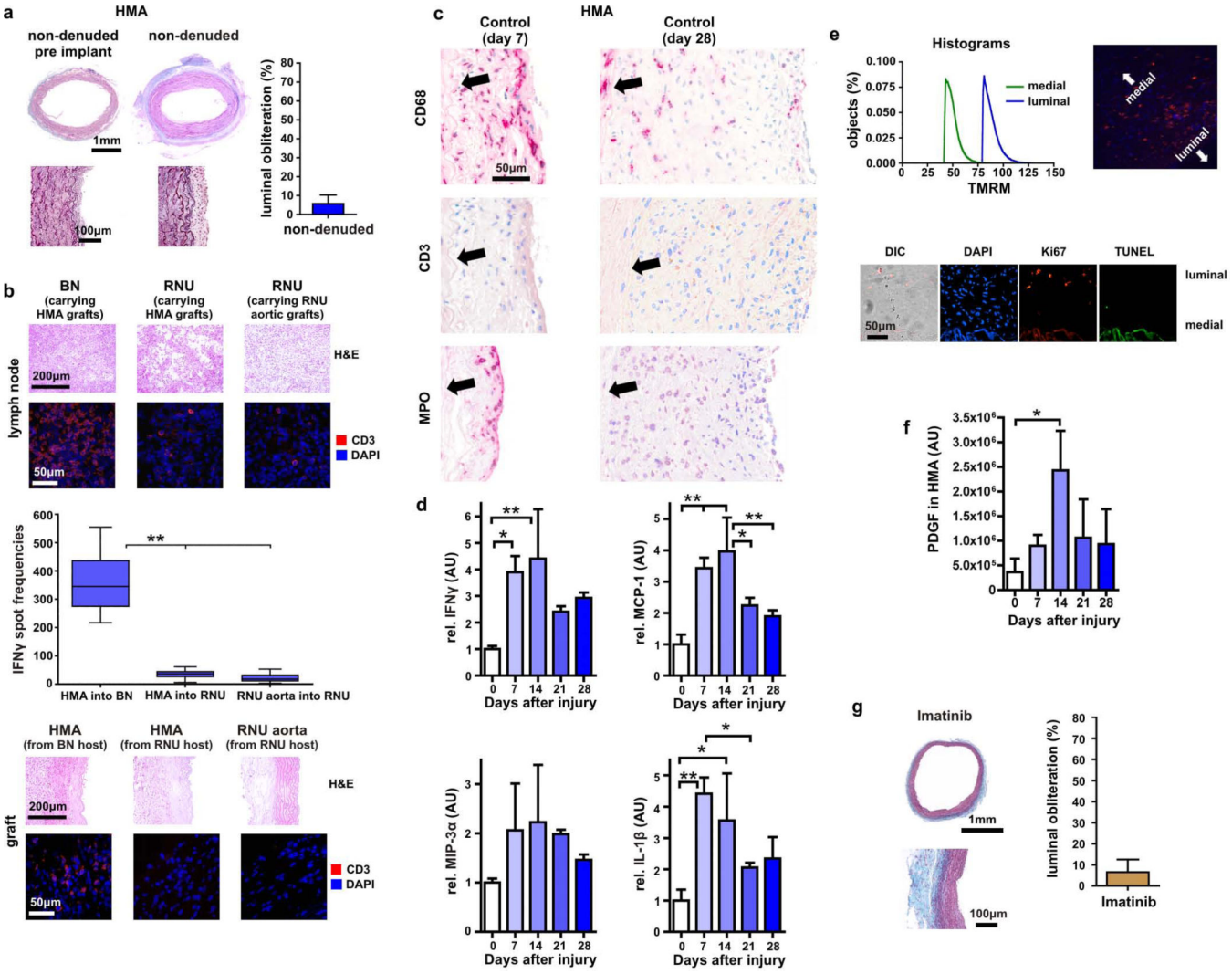

Extended Data Figure 3. The central role for PDGF in advancing myointima formation

a, After 28 days, non-denuded HMAs in RNU rats showed only minor myointimal lesions (trichrome, mean ± s.d., n = 5 animals). **b**, To evaluate a possible rejection process in the xenogeneic HMA setting, host immune activation and graft infiltration were assessed. In the HMA model, xenogeneic HMA were transplanted into RNU rats (middle column). Xenogeneic HMA transplants into immunocompetent hosts (Brown Norway rats; BN, left column) and syngeneic RNU aortic transplants into RNU recipients (right column) served as controls; all analyses were performed after 7 days. Para-aortic BN lymph nodes harboured huge amounts of $CD3^+$ lymphocytes, whereas the number was low in RNU lymph nodes. In IFNγ-Elispot assays with homogenized graft cells and recipient splenocytes, only BN

recipients showed strong immune activation, whereas RNU recipients failed to mount a relevant immune response (box 25th to 75th percentile with median, whiskers min–max, quadruplicates of 5 animals (columns 1 and 2) and 4 animals (column 3), ANOVA with Bonferroni's post-hoc test). Dense $CD3^+$ infiltrates were found in HMA grafts of BN recipients, but not in HMA or RNU aortic grafts in RNU recipients. **c**, Immunohistochemistry identified myointimal macrophages and neutrophils in HMA control specimens on day 7 and reduced leukocyte infiltration in control specimens on day 28. Lymphocytes were not observed (black arrows, internal elastic lamina). **d**, HMA tissue levels of the inflammatory cytokines IFNγ, MCP-1, MIP-3α, and IL-1β were elevated during the first 14 days (mean ± s.d., $n = 3$ animals per group, ANOVA with Bonferroni's post-hoc test). **e**, In HMA day 21 vessels, spatial differences of SMC ΔΨm with higher TMRM fluorescence in the luminal areas compared to the areas adjacent to the media were observed. SMC proliferation also mainly occurred in these luminal regions of elevated ΔΨm. DIC, differential interference contrast. **f**, Tissue PDGF was increased in HMA after injury and peaked after 14 days (mean ± s.d., $n = 3$ animals per time point, ANOVA with Bonferroni's post-hoc test). **g**, Compared to untreated control vessels at day 28 in the rat aortic balloon injury model (Extended Data Fig. 1g), imatinib (PDGF-R blocker)-treated 28-day vessels showed only minor lesions (mean ± s.d., $n = 8$ animals). $^*P < 0.05$; $^{**}P < 0.01$.

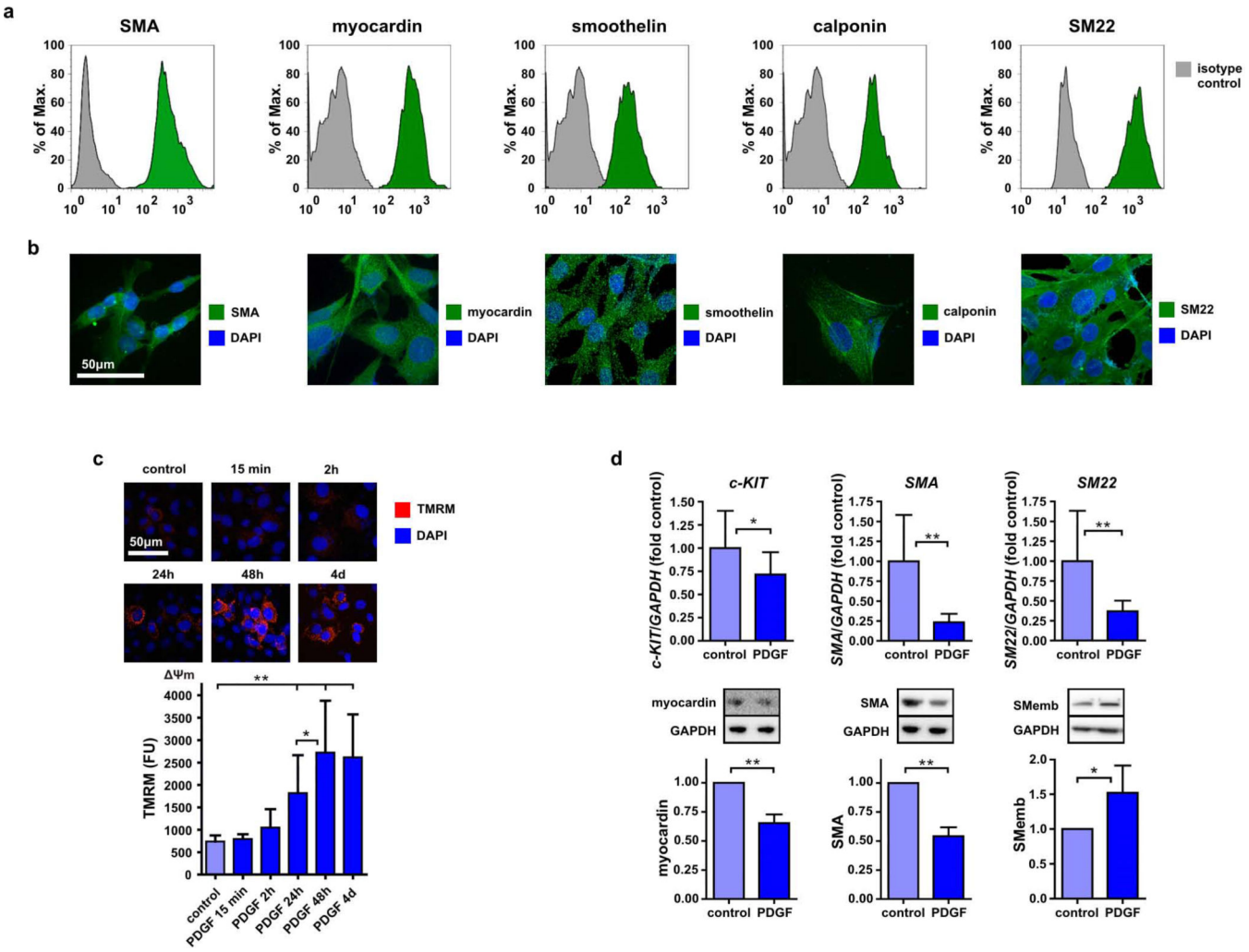

Extended Data Figure 4. SMC characterization and response to PDGF

a, **b**, Cells isolated from fresh HMA were positive for SMA, myocardin, smoothelin, calponin, and SM22α (SM22) as detected by FACS (**a**, pictures are representative of three replicates) and immunofluorescence (**b**, pictures are representative of three replicates). Thus, cells were identified as SMCs, but we cannot rule out that cells from other sources (for example, vessel wall stem cells with smooth muscle characteristics) were also involved. **c**, ΔΨm hyperpolarization, a phenomenon observed at times of maximized net proliferative activity in HMA (Fig. 1f), could be linked to PDGF. When SMCs were incubated with PDGF, ΔΨm hyperpolarization steadily increased over time, reaching its maximum after 48 h (mean ± s.d., 5 replicates of 2 (15 min, 2 h) or 3 (all other groups) independent experiments, ANOVA with Bonferroni's post-hoc test). **d**, We found a significant downregulation of *c-KIT*, *SMA* and *SM22* mRNA versus *GAPDH* mRNA after incubation with PDGF, all maturity markers for contractile SMCs (mean ± s.d., 13 independent experiments, Student's *t*-test). Western blot analysis further revealed a downregulation of myocardin and confirmed SMA reduction. In contrast, SMemb, the embryonic form of smooth muscle myosin heavy chain and a marker for dedifferentiated SMCs, was increased, indicating a PDGF-induced phenotype switch (mean ± s.d., 5 (myocardin and SMA) and 6

(SMemb) independent experiments, PDGF normalized to control, one-sample *t*-tests). *P < 0.05; **P < 0.01.

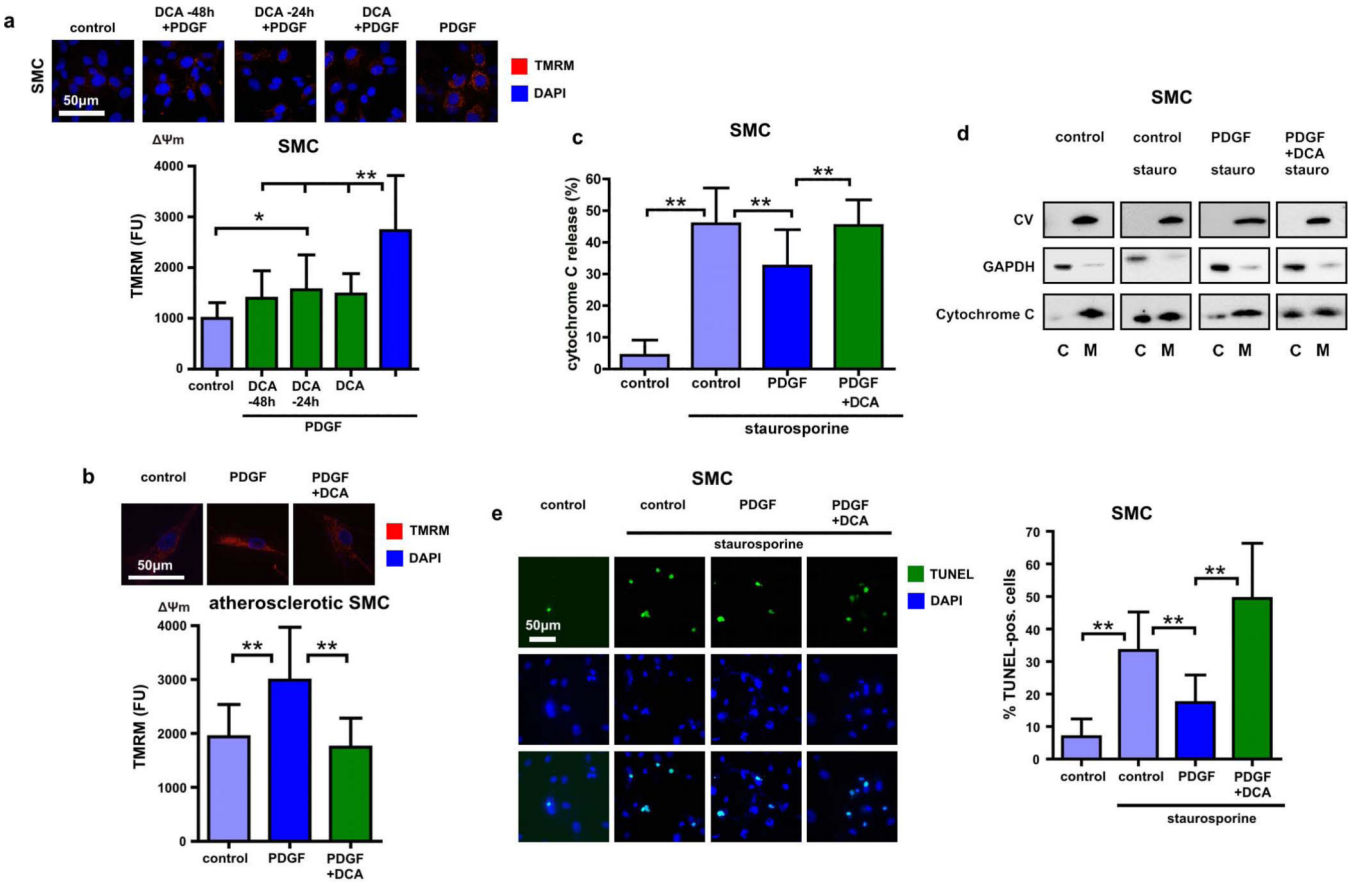

Extended Data Figure 5. DCA reduces ΔΨm hyperpolarization and facilitates apoptosis in SMCs

a, To assess the kinetics of DCA action *in vitro*, SMCs were pre-incubated with DCA for different time periods and then stimulated with PDGF for 48 h (mean ± s.d., 10 replicates of 3 independent experiments per group, ANOVA with Bonferroni's post-hoc test). DCA reduced PDGF-induced ΔΨm hyperpolarization irrespective of the pre-incubation period. **b**, Atherosclerotic plaques from heavily calcified and atherosclerotic human coronary arteries were scraped off the media and cultured in SMC medium. Outgrowing SMCs were picked and expanded. PDGF significantly increased ΔΨm, an effect that was prevented by DCA (mean ± s.d., 10 replicates of 3 independent experiments, ANOVA with Bonferroni's post-hoc test). **c–e**, Apoptosis induction with staurosporine significantly increased the number of control SMCs that showed cytochrome C leakage, as identified by diffuse cytochrome C staining throughout the cell (**c**, mean ± s.d., 10 replicates of 2 independent experiments per group, ANOVA with Bonferroni's post-hoc test). PDGF significantly reduced cytochrome C release in SMCs and DCA counteracted this PDGF effect. Cytoplasmatic (C) and mitochondrial fractions (M) were isolated for immunoblotting (**d**, data are representative of 3 independent experiments). Separation was confirmed by the contents of mitochondrial complex V (CV) and cytosolic GAPDH. Cytochrome C was retained inside the mitochondria in control SMCs and was released with staurosporine. PDGF reduced the

cytoplasmatic fraction, indicating reduced cytochrome C release, and DCA reversed the PDGF effect. SMC apoptosis was detected by TUNEL staining (**e**, mean ± s.d., 10 replicates of 2 (column 1) or 3 (columns 2–4) independent experiments, ANOVA with Bonferroni's post-hoc test). Staurosporine significantly increased the number of apoptotic control SMCs. PDGF treatment decreased the percentage of apoptotic SMCs and DCA reversed this anti-apoptotic effect. *$P < 0.05$; **$P < 0.01$.

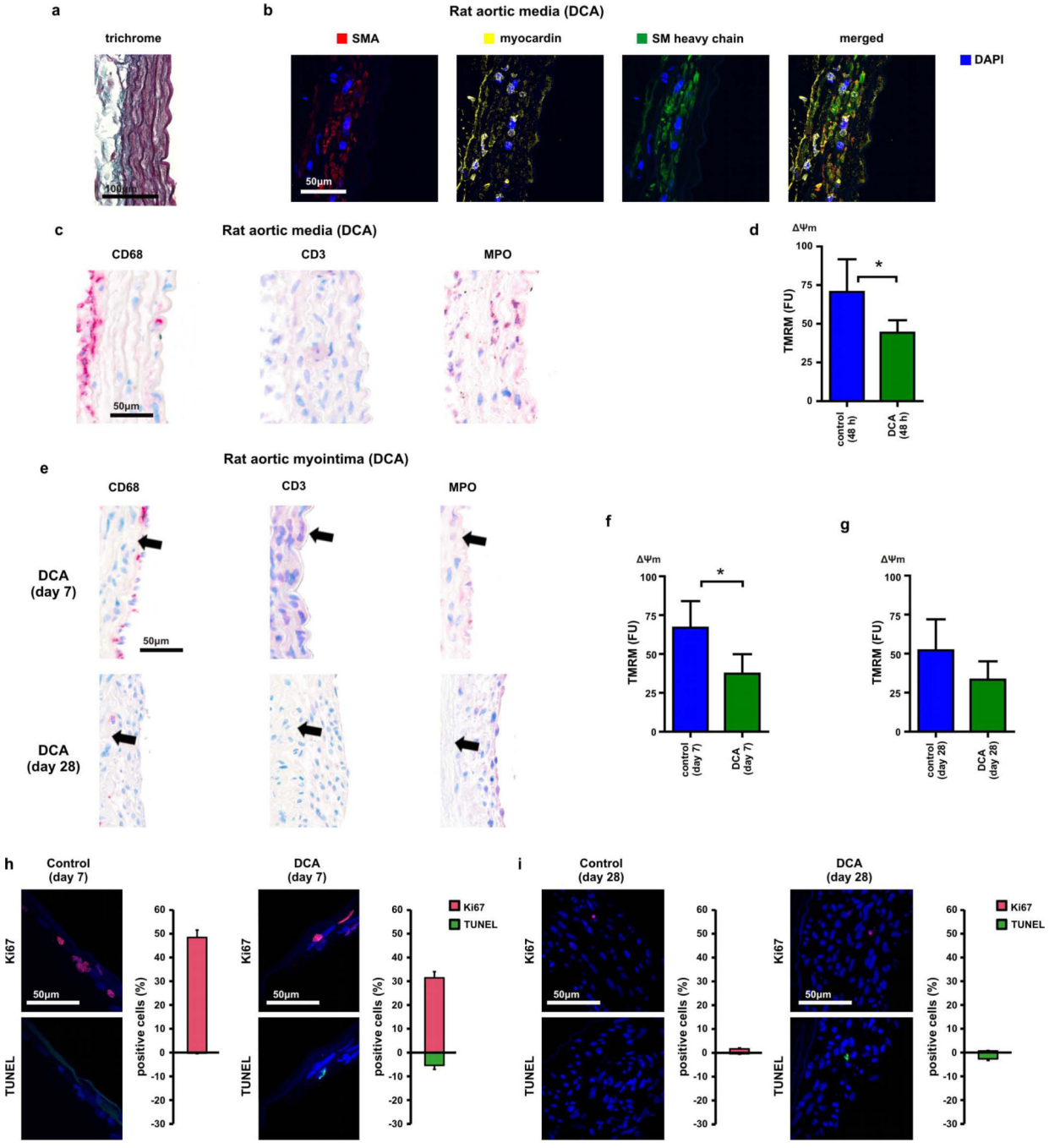

Extended Data Figure 6. DCA lowers medial and myointimal ΔΨm and facilitates apoptosis in balloon-injured rat aortas

a, **b**, Trichrome (**a**) and immunofluorescence (**b**) confirmed abundant SMCs in the aortic media of DCA-treated animals 48h after injury. **c**, Similar to control vessels, the infiltrate mainly contained macrophages and neutrophils, but no $CD3^+$ lymphocytes. **d**, DCA reduced ΔΨm of medial cells (mean ± s.d., $n = 6$ animals (control at 48 h) and 4 animals (DCA at 48 h), Student's *t*-test). **e**, Macrophages were the main inflammatory cell population in the developing myointima of immunocompetent DCA animals at 7 days. Very few neutrophils and no lymphocytes were observed. Leukocyte infiltration was markedly alleviated at 28 days (black arrows, internal elastic lamina). **f**, **g**, DCA effectively lowered the elevated ΔΨm of myointimal cells on day 7 (**f**, mean ± s.d., $n = 4$ animals per group, Student's *t*-test), but had little effect on the already reduced ΔΨm at 28 days (**g**, mean ± s.d., $n = 6$ animals per group, Student's *t*-test). **h**, **i**, The percentages of proliferating ($Ki67^+$) and apoptotic ($TUNEL^+$) cells in the myointima were calculated (representative cropped pictures of the myointima are presented). The few myointimal cells in control- and DCA-vessels at 7 days showed high proliferative activity (red, positive *y* axis), but apoptosis (green, negative *y* axis) was only observed in DCA-treated animals (**h**, mean ± s.e.m., $n = 4$ animals per group). Proliferation and apoptosis were low after 28 days in both groups (**i**, mean ± s.e.m., $n = 5$ animals (control at day 28) and 7 animals (DCA at day 28)). $^*P < 0.05$.

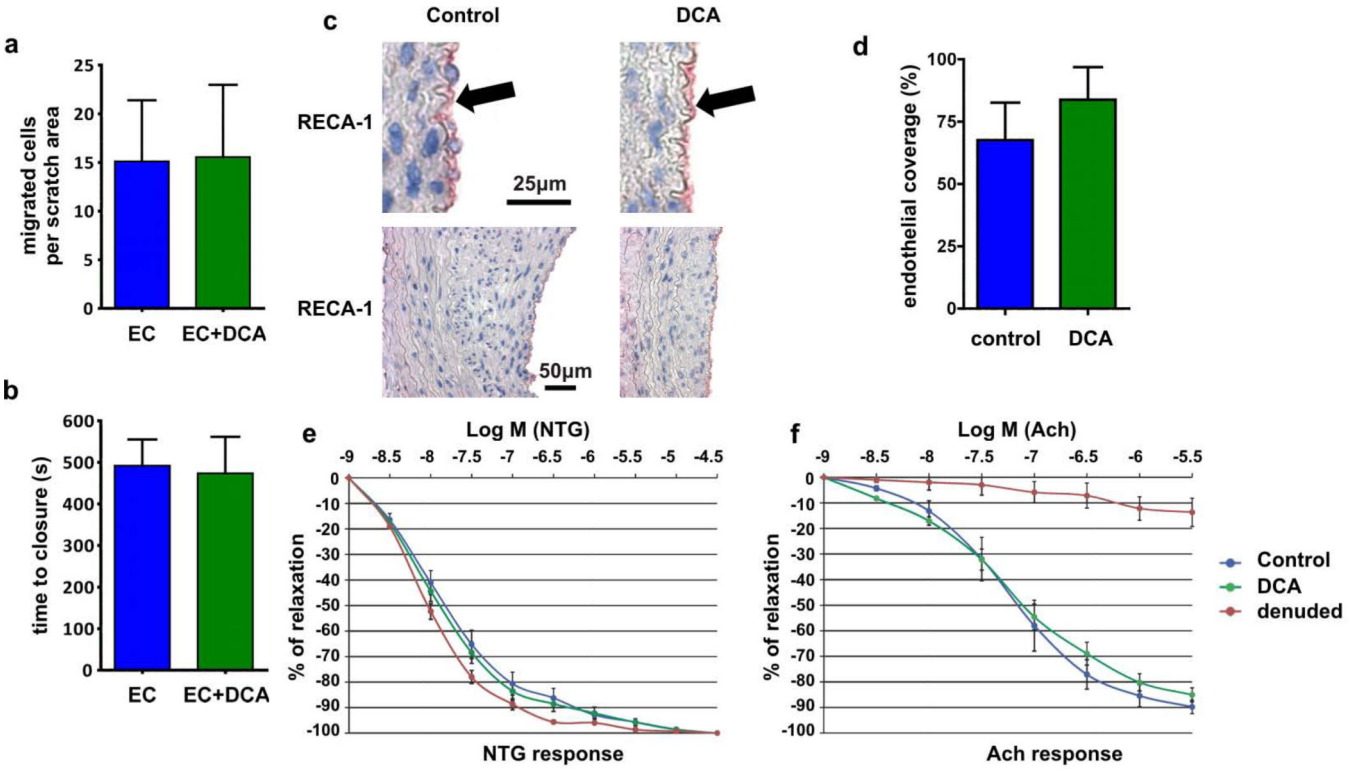

Extended Data Figure 7. DCA does not impair endothelial cell migration or vessel re-endothelialization

The effect of DCA on endothelial cell (EC) migration was assessed *in vitro*. **a**, **b**, A scratch (width 338 µm) was made across a confluent human EC monolayer. The number of cells that migrated into a 340 µm × 338 µm scratch rectangle within 5 h was counted (**a**, mean ± s.d., triplicates of 3 independent experiments, Student's *t*-test) and the time needed to close

the scratch was recorded (**b**, mean ± s.d., *n* = 5 (EC), 4 (EC + DCA) independent experiments, Student's *t*-test). There were no differences between untreated and DCA-treated ECs. **c**, **d**, To evaluate vessel re-endothelialization, rat aortas underwent mechanical endothelial denudation by balloon injury. Aortas were recovered after 28 days and stained for rat endothelial cell antigen (**c**, black arrows, RECA-1). Re-endothelialization was quantified (**d**, mean ± s.d., *n* = 5 animals (control at day 28) and 6 animals (DCA at day 28), Student's *t*-test) and was similar in both groups. **e**, **f**, Endothelial function in both 28-day groups was further assessed in relaxation studies and compared to denuded aortas three days after balloon injury (mean ± s.e.m., *n* = 9 animals (control at day 28), 11 animals (DCA at day 28) and 3 animals (denuded at day 3)). Freshly recovered aortic segments were pre-constricted and DCA-treated and control vessels, as well as denuded aortas, showed similar endothelium-independent relaxation capacities using nitroglycerin (NTG) as vasodilator (**e**). However, denuded aortas largely failed to show endothelium-dependent relaxation with acetylcholine (Ach; **f**). Both DCA-treated and control vessels demonstrated similar and physiologic endothelium-dependent relaxation, indicating functional integrity of the vascular endothelium.

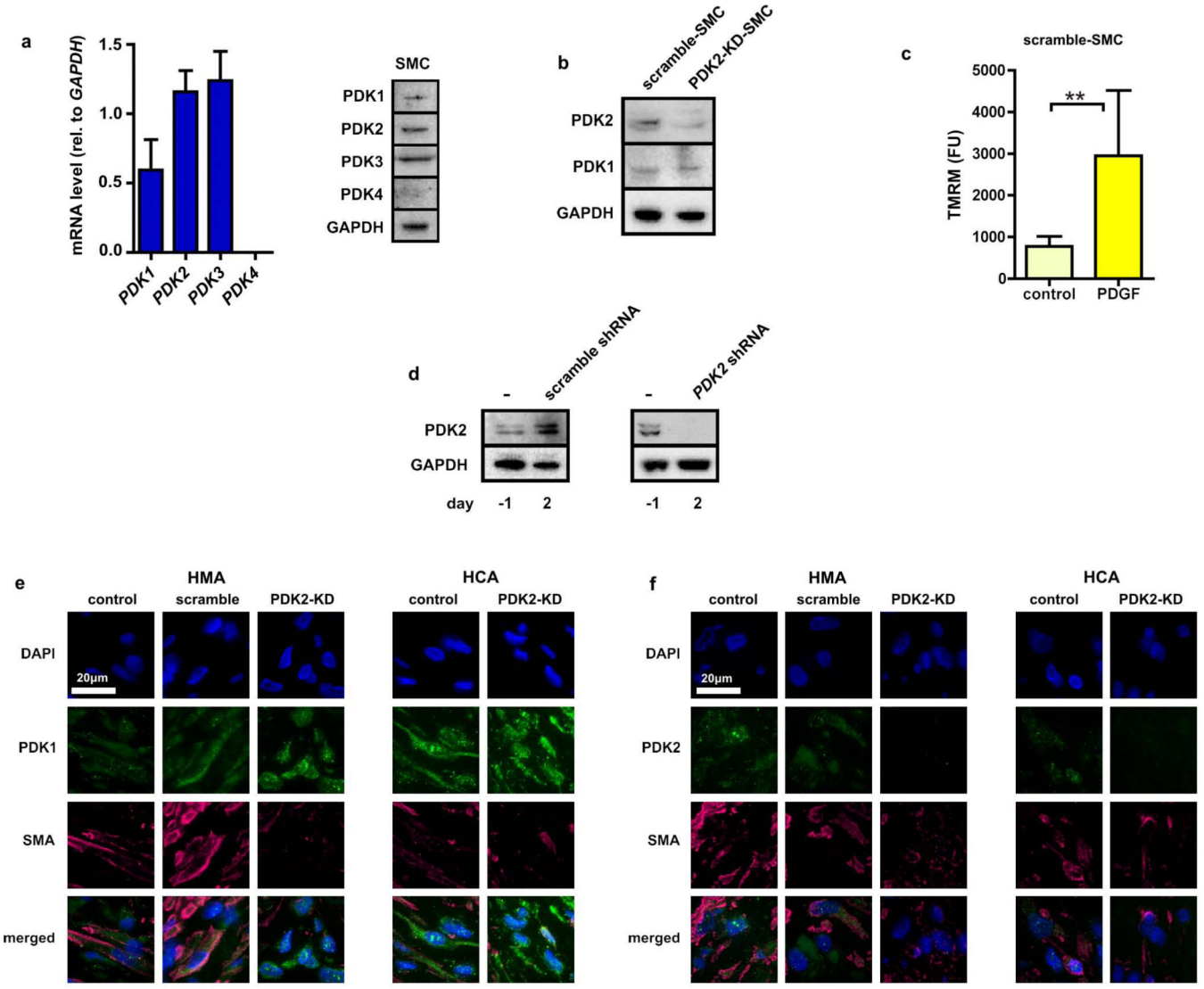

Extended Data Figure 8. PDK2 knockdown in SMCs, HMAs and HCAs

a, *PDK1*, *PDK2*, *PDK3* and *PDK4* mRNA expression was assessed in control SMCs and normalized to *GAPDH* (mean ± s.d., 3 independent experiments). *PDK1*, *PDK2* and *PDK3* mRNA was detected as shown. Also, PDK1, PDK2 and PDK3 but not PDK4 were detectable in immunoblot analyses (data are representative of 3 independent experiments). **b**, To confirm *in vitro* PDK2 knockdown, PDK1 and PDK2 expressions were assessed in immunoblot analyses (data are representative of 3 independent experiments). PDK2 was markedly reduced in PDK2-knockdown SMCs (PDK2-KD-SMC), but not in scramble shRNA-transduced SMCs (scramble-SMC). PDK1 expression remained unaffected by *PDK2*- or scramble-shRNA constructs. **c**, To exclude that lentiviral shRNA transduction changed the ΔΨm response to PDGF, scramble-SMCs were stimulated with PDGF (mean ± s.d., 10 replicates of 2 independent experiments, Student's *t*-test). Both the baseline potential and the PDGF-triggered increase in ΔΨm were similar to SMCs (see Extended Data Fig. 5a). **d**, Fresh HMA vessels underwent balloon injury, were divided, and one half was sampled (day -1). The other half was incubated with lentiviral particles containing *PDK2* or

scrambled shRNA. On the next day, transduced vessels were transplanted into RNU rats. Two days later, vessels were recovered (day 2) for immunoblotting. PDK2 could be detected in untreated HMA vessels (day -1). On day 2, only scrambled control HMAs, but not PDK2-KD vessels showed a PDK2 signal (data are representative of 3 independent experiments). **e**, **f**, After 28 days, HMA and HCA samples were stained for DAPI, PDK1, PDK2 and SMA. PDK1 was similarly detectable in all control, scramble and PDK2-KD sections at day 28 (**e**, pictures are representative of 3 independent experiments). At day 28, HMA control and scramble as well as HCA control showed detectable PDK2 protein, whereas PDK2 fluorescence in HMA and HCA PDK2-KD at day 28 was negligible (**f**, pictures are representative of 3 independent experiments), demonstrating selective knockdown. $^{**}P < 0.01$.

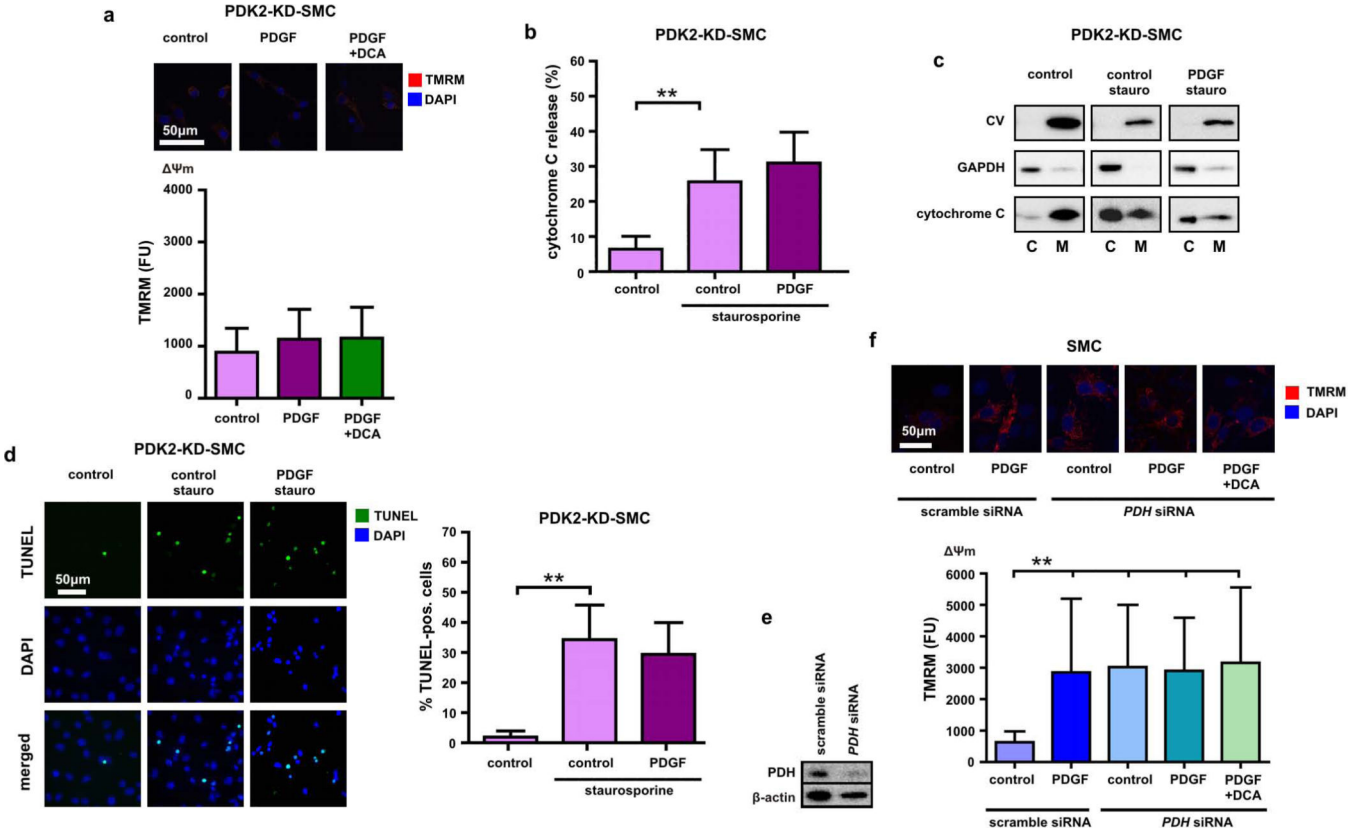

Extended Data Figure 9. PDK2 knockdown mimics the DCA effect on SMC ΔΨm and apoptosis

a, PDK2-KD-SMCs were pre-incubated with DCA and/or stimulated with PDGF. PDK2-KD-SMCs maintained low ΔΨm despite PDGF stimulation and DCA did not further depolarize ΔΨm (mean ± s.d., 10 replicates of 3 (columns 1 and 3) or 4 (column 2) independent experiments, ANOVA with Bonferroni's post-hoc test). **b**, **c**, Apoptosis was induced with staurosporine. Control PDK2-KD-SMCs showed mainly mitochondria-housed cytochrome C in fluorescence stainings (**b**, mean ± s.d., 10 replicates of 2 independent experiments, ANOVA with Bonferroni's post-hoc test) and compartment-separated immunoblot analyses (**c**, data are representative of 2 independent experiments). After induction of apoptosis, cytochrome C leaked into the cytoplasm and PDGF did not suppress

cytochrome C leakage. **d**, PDGF did not induce resistance to apoptosis in PDK2-KD-SMCs (mean ± s.d., 10 replicates of 2 independent experiments per group, ANOVA with Bonferroni's post-hoc test). **e**, To establish a link between PDH and ΔΨm, PDH was knocked down (data are representative of 2 independent experiments). **f**, ΔΨm was significantly increased in *PDH* siRNA-transfected SMCs and PDGF and DCA no longer affected ΔΨm (mean ± s.d., 10 replicates of 2 (column 2) or 3 (columns 1, 3, 4 and 5) independent experiments, ANOVA with Bonferroni's post-hoc test). $^{**}P < 0.01$.

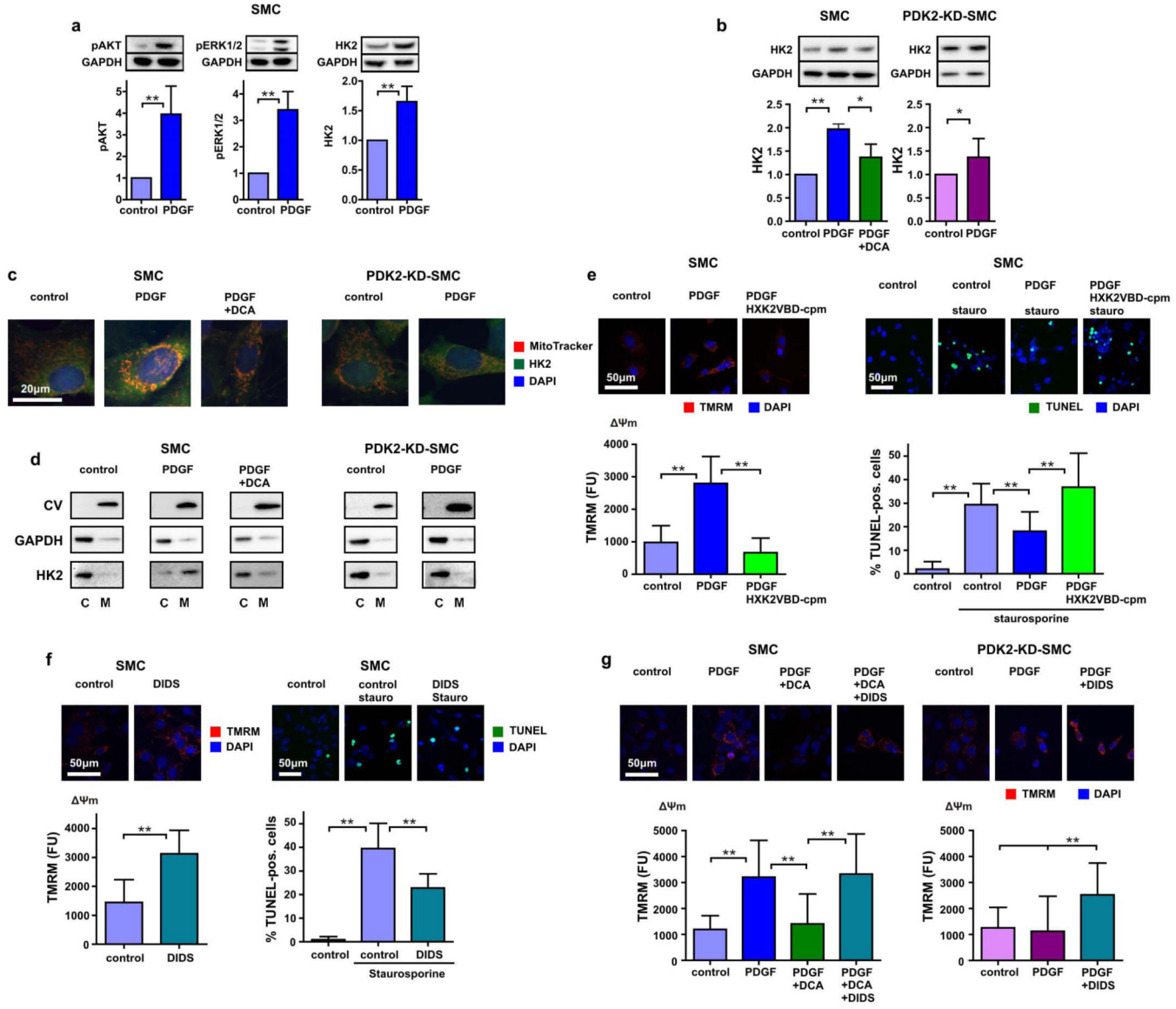

Extended Data Figure 10. VDAC controls ΔΨm and apoptosis

a, PDGF stimulation of SMCs significantly increased phosphorylated AKT, and ERK1 and ERK2, and increased the expression of HK2 (mean ± s.d., 5 (pAKT and pERK1/2) and 8 (HK2) independent experiments, PDGF normalized to control, one-sample *t*-tests). **b**, Immunoblot analysis revealed PDGF-induced upregulation of HK2 expression in SMCs

(mean ± s.d., 3 (SMC) independent experiments, data normalized to control, one-sample *t*-test (control versus PDGF), Student's *t*-test (PDGF versus PDGF + DCA)). HK2 upregulation was alleviated by DCA or PDK2-KD (mean ± s.d., 8 (PDK2-KD-SMC) independent experiments, PDGF normalized to control, one-sample *t*-test). **c**, Confocal images with mitochondrial (MitoTracker, red), HK2 (green), and nuclear staining (DAPI, blue, data are representative of 2 independent experiments) were captured. Co-localization of green HK2 with red mitochondria generated a yellow colour. SMCs incubated with PDGF increased their yellow signal, an effect that was prevented by DCA. PDGF did not induce HK2-mitochondrial association in PDK2-KD-SMCs. **d**, Cytoplasmatic (C) and mitochondrial fractions (M) were isolated for immunoblotting (data are representative of 2 independent experiments). In control SMCs and PDK2-KD-SMCs, HK2 was mainly detected in the cytoplasmatic fraction. In SMCs, PDGF caused a partial translocation of HK2 to the mitochondrial compartment. DCA markedly alleviated this translocation. PDGF did not induce HK2 translocation in PDK2-KD-SMCs. **e**, In the presence of HXK2VBD-cpm, PDGF failed to induce both ΔΨm hyperpolarization (mean ± s.d., 10 replicates of 3 independent experiments, ANOVA with Bonferroni's post-hoc test) and apoptosis resistance (mean ± s.d., 10 replicates of 3 independent experiments, ANOVA with Bonferroni's post-hoc test). **f**, VDAC inhibition by DIDS caused ΔΨm hyperpolarization (mean ± s.d., 10 replicates of 2 independent experiments, Student's *t*-test) and rendered SMCs resistant to staurosporine-induced apoptosis (mean ± s.d., 10 replicates of 3 independent experiments, ANOVA with Bonferroni's post-hoc test). **g**, The depolarizing effect of DCA on PDGF-treated SMCs was counteracted by DIDS (mean ± s.d., 10 replicates of 3 independent experiments, ANOVA with Bonferroni's post-hoc test). Although PDGF did not increase ΔΨm in PDK2-KD-SMC, DIDS caused marked mitochondrial hyperpolarization (mean ± s.d., 10 replicates of 2 independent experiments, ANOVA with Bonferroni's post-hoc test). $*P < 0.05$; $**P < 0.01$.

Supplementary Material

Refer to Web version on PubMed Central for supplementary material.

Acknowledgements

We thank C. Pahrmann for performing all cell cultures and for her technical assistance. We thank J. Thoms for performing immunoblots, H. Wiebold for assistance in organ chamber experiments, J. Lyons and her team for her assistance with the swine study, and S. Ehret, A. Deng and M. Resch for their technical assistance. We thank the UKE Imaging Facility (UMIF, B. Zobiak) and the UKE Animal Facility. Ethicon (Norderstedt, Germany) provided surgical suture materials. We also thank A. Treszl and G. Schoen for their statistical analyses. This study was funded by the German Research Foundation (Deutsche Forschungsgemeinschaft (DFG), SCHR992/3-1 and SCHR992/4-1 to S.S.), the International Society for Heart and Lung Transplantation (ISHLT, to S.S.), the Förderverein des Universitären Herzzentrums Hamburg (to S.S.), the Hermann and Lilly Schilling Foundation (to C.K.), the MINECO (SAF2013-41177-R, to J.P.B.) and the NIH (NIH 1R01HL105299, to P.S.T.).

References

1. Lloyd-Jones D, et al. Heart disease and stroke statistics—2009 update: a report from the American Heart Association Statistics Committee and Stroke Statistics Subcommittee. Circulation. 2009; 119:480–486. [PubMed: 19171871]
2. Dzau VJ, Braun-Dullaeus RC, Sedding DG. Vascular proliferation and atherosclerosis: new perspectives and therapeutic strategies. Nature Med. 2002; 8:1249–1256. [PubMed: 12411952]

3. Novak K. Cardiovascular disease increasing in developing countries. Nature Med. 1998; 4:989–990. [PubMed: 9734376]
4. Green DR, Reed JC. Mitochondria and apoptosis. Science. 1998; 281:1309–1312. [PubMed: 9721092]
5. Hengartner MO. The biochemistry of apoptosis. Nature. 2000; 407:770–776. [PubMed: 11048727]
6. Zamzami N, Kroemer G. The mitochondrion in apoptosis: how Pandora's box opens. Nature Rev. Mol. Cell Biol. 2001; 2:67–71. [PubMed: 11413468]
7. Halestrap AP. What is the mitochondrial permeability transition pore? J. Mol. Cell. Cardiol. 2009; 46:821–831. [PubMed: 19265700]
8. Bonnet S, et al. A mitochondria–K^+ channel axis is suppressed in cancer and its normalization promotes apoptosis and inhibits cancer growth. Cancer Cell. 2007; 11:37–51. [PubMed: 17222789]
9. Bernardi P. Modulation of the mitochondrial cyclosporin A-sensitive permeability transition pore by the proton electrochemical gradient. Evidence that the pore can be opened by membrane depolarization. J. Biol. Chem. 1992; 267:8834–8839. [PubMed: 1374381]
10. Roche TE, Hiromasa Y. Pyruvate dehydrogenase kinase regulatory mechanisms and inhibition in treating diabetes, heart ischemia, and cancer. Cell. Mol. Life Sci. 2007; 64:830–849. [PubMed: 17310282]
11. Azoulay-Zohar H, Israelson A, Abu-Hamad S, Shoshan-Barmatz V. In self-defence: hexokinase promotes voltage-dependent anion channel closure and prevents mitochondria-mediated apoptotic cell death. Biochem. J. 2004; 377:347–355. [PubMed: 14561215]
12. Pastorino JG, Shulga N, Hoek JB. Mitochondrial binding of hexokinase II inhibits Bax-induced cytochrome c release and apoptosis. J. Biol. Chem. 2002; 277:7610–7618. [PubMed: 11751859]
13. Clarke MC, et al. Apoptosis of vascular smooth muscle cells induces features of plaque vulnerability in atherosclerosis. Nature Med. 2006; 12:1075–1080. [PubMed: 16892061]
14. Bernal-Mizrachi C, et al. Vascular respiratory uncoupling increases blood pressure and atherosclerosis. Nature. 2005; 435:502–506. [PubMed: 15917810]
15. Mitra AK, Del Core MG, Agrawal DK. Cells, cytokines and cellular immunity in the pathogenesis of fibroproliferative vasculopathies. Can. J. Physiol. Pharmacol. 2005; 83:701–715. [PubMed: 16333372]
16. Newby AC, Zaltsman AB. Molecular mechanisms in intimal hyperplasia. J. Pathol. 2000; 190:300–309. [PubMed: 10685064]

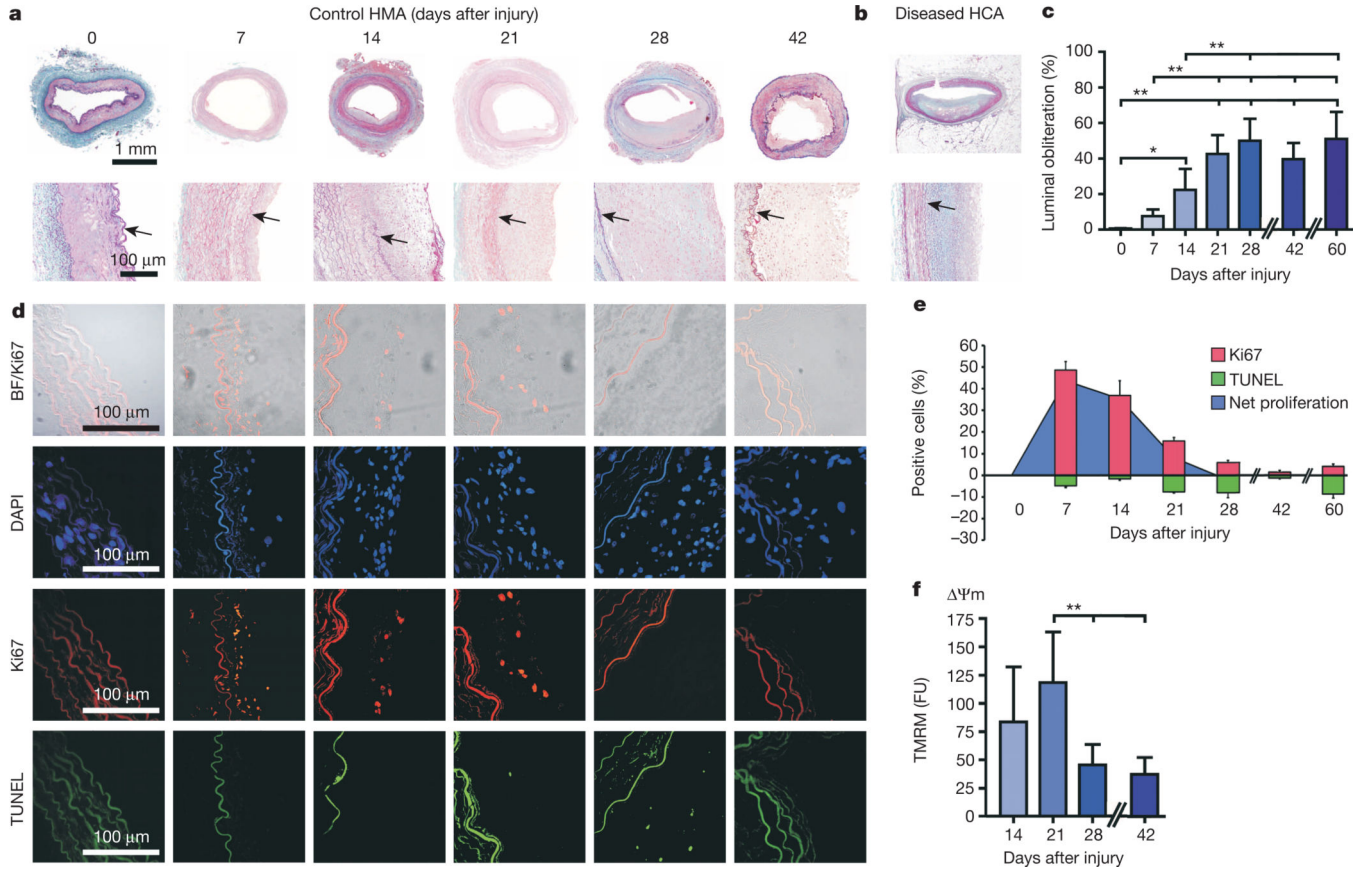

Figure 1. Chronology and growth dynamics of myointima formation in the HMA model

a, Development of myointimal hyperplasia (trichrome; black arrows, internal elastic lamina). **b**, Non-calcified lesions in naturally diseased human coronary artery (HCA). **c**, Luminal obliteration over time (mean ± s.d., n = 5 animals (days 0–28), 4 animals (days 42–60), ANOVA with Bonferroni's post-hoc test). **d**, **e**, The timeline of proliferative (Ki67) and apoptotic activity (TUNEL, TdT-mediated dUTP nick end labelling) within the myointima was monitored by immunofluorescence (**d**) and quantified (**e**, mean ± s.e.m., n = 7 animals (day 7), 5 animals (day 14), 6 animals (days 21–60)). Net proliferation was calculated as the percentage of Ki67-positive minus TUNEL-positive cells. BF, brightfield. **f**, ΔΨm in HMA myointima (mean ± s.d., n = 5 animals (day 14), 9 animals (day 21), 6 animals (days 28–42), ANOVA with Bonferroni's post-hoc test). FU, arbitrary fluorescence units; TMRM, tetramethylrhodamine methyl ester perchlorate assay. *P < 0.05, **P < 0.01.

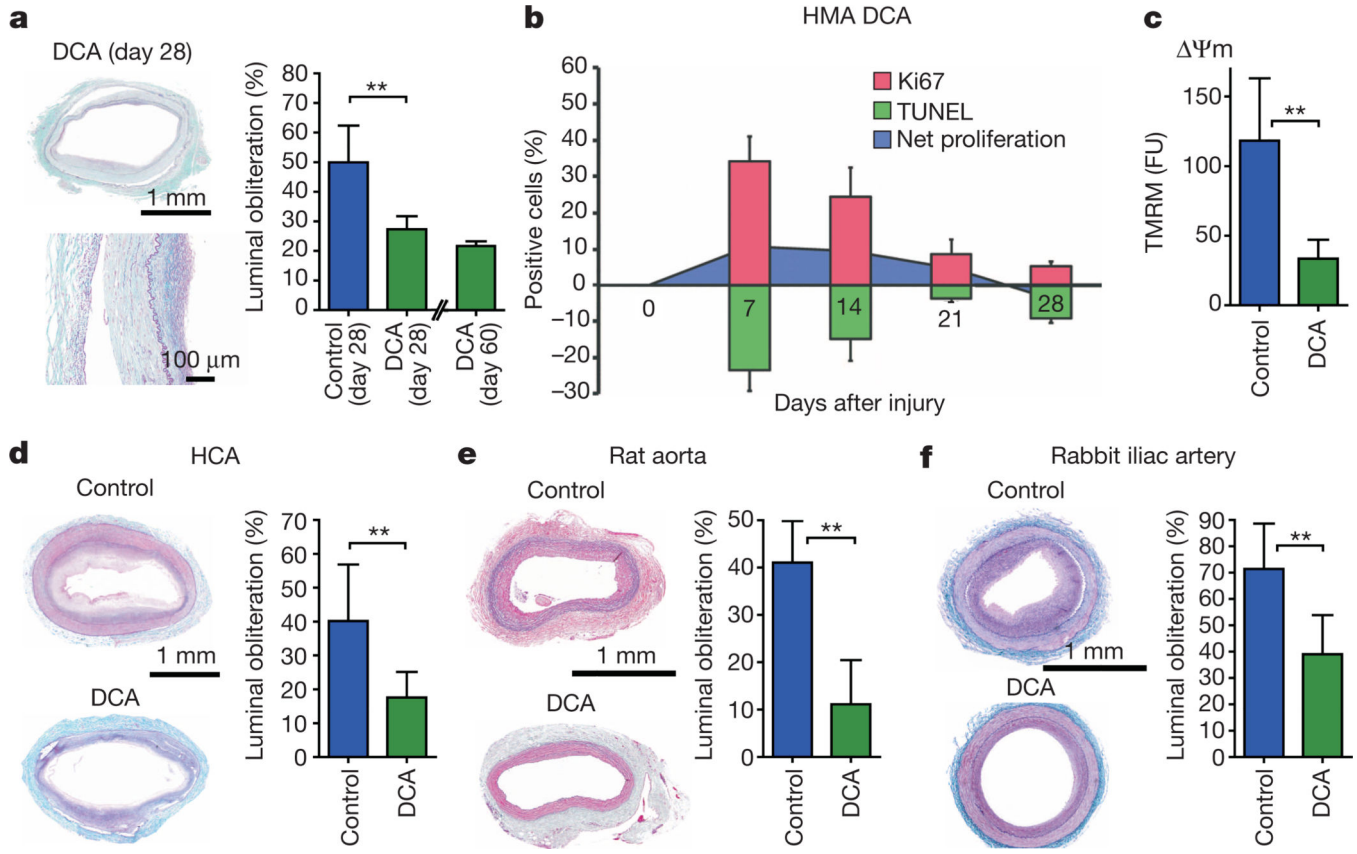

Figure 2. DCA alleviates myointima formation *in vivo*

a, After 28 days, luminal obliteration was significantly less in the DCA group of the HMA model (mean ± s.d., $n = 5$ animals per group, Student's *t*-test). In animals treated for 60 days ($n = 4$), there was no further disease progression. **b**, Myointimal growth dynamics in the HMA DCA group (mean ± s.e.m., $n = 4$ animals (day 7), 5 animals (day 14), 3 animals (day 21), 6 animals (day 28)). **c**, At day 21, ΔΨm was significantly lower in HMA DCA vessels than in control arteries (mean ± s.d., $n = 9$ control animals, $n = 4$ DCA animals, Student's *t*-test). **d**, At day 28, DCA reduced luminal obliteration in the HCA model (mean ± s.d., $n = 8$ control animals, $n = 14$ DCA animals, Student's *t*-test). **e**, **f**, At day 28, DCA effectively alleviated myointima formation in balloon-injured rat aortas (**e**, mean ± s.d., $n = 6$ animals per group, Student's *t*-test) and rabbit iliac arteries (**f**, mean ± s.d., $n = 12$ control animals, $n = 15$ DCA animals, Student's *t*-test). $^{**}P < 0.01$.

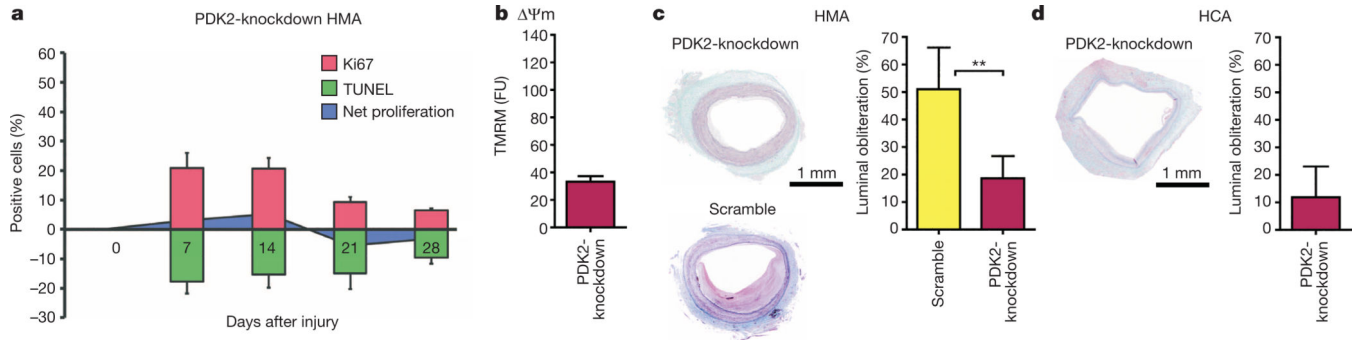

Figure 3. PDK2 knockdown alleviates myointima formation *in vivo*

a, PDK2-knockdown HMAs showed elevated apoptosis rates during the early time points of increased proliferative activity resulting in low myointimal net proliferation (mean ± s.e.m., $n = 3$ (day 7), 4 (day 14), 3 (day 21), 8 (day 28) animals). **b**, At day 21, ΔΨm in PDK2-knockdown HMA vessels was approximately as low as in DCA HMA vessels (mean ± s.d., $n = 4$ animals; see Fig. 2c). **c**, At day 28, luminal obliteration was significantly reduced in PDK2-knockdown HMA compared to scrambled shRNA controls (mean ± s.d., $n = 4$ animals (scramble) and $n = 9$ animals (PDK2-knockdown, Student's *t*-test). **d**, Luminal obliteration was low in PDK2-knockdown HCA vessels at day 28 (mean ± s.d., $n = 3$ animals). $^{**}P < 0.01$.

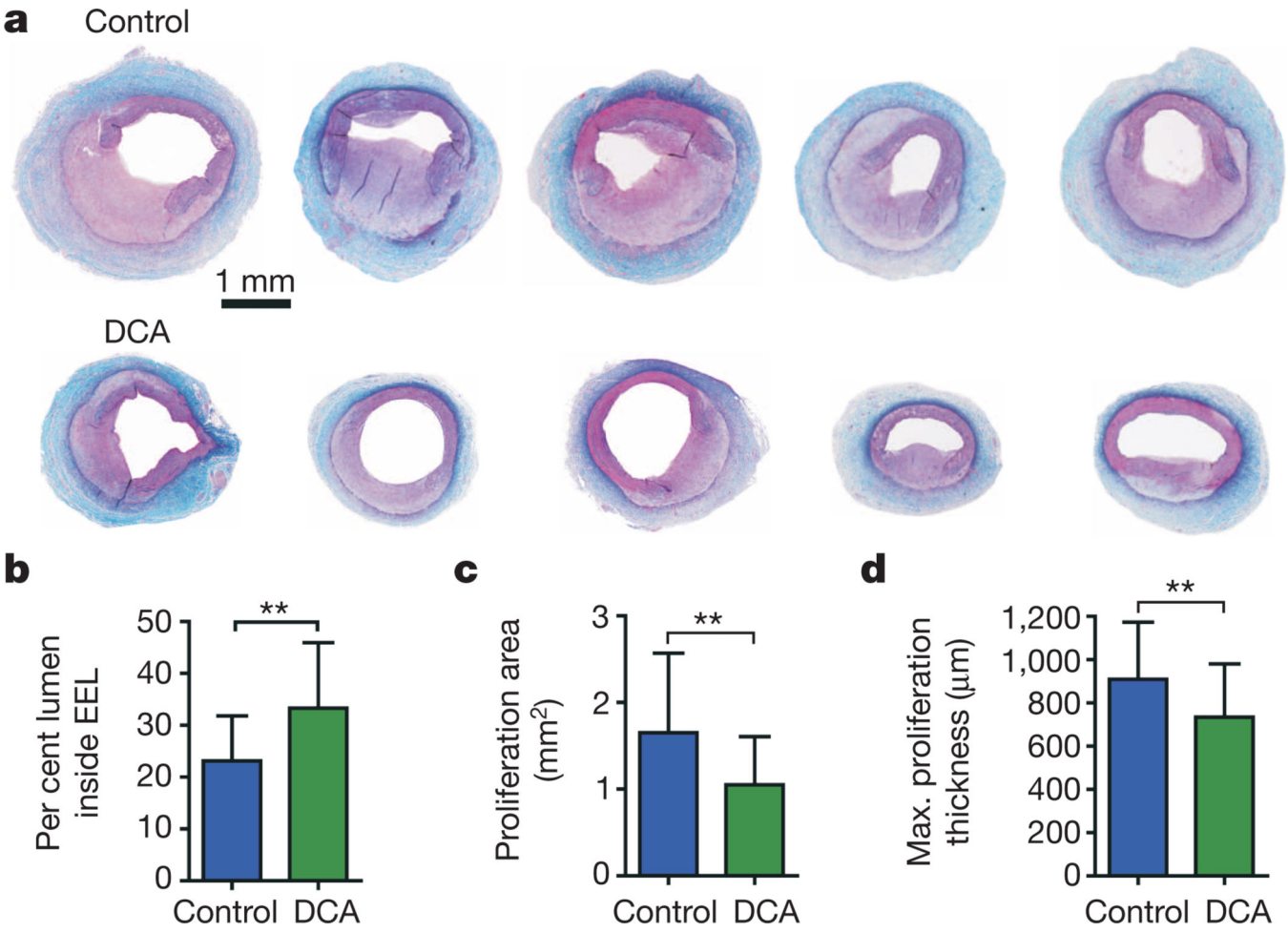

Figure 4. DCA effectively reduces balloon-injury-induced myointima formation in swine coronary arteries *in vivo*

a, After 28 days, the coronary arteries of untreated and DCA-treated Yorkshire swine were retrieved (trichrome). One representative vessel per animal is presented. **b**, The patent lumen inside the external elastic lamina (EEL) was significantly larger in the DCA group (mean ± s.d., $n = 45$ sections per group (three sections per vessel, three coronary arteries per pig, five pigs per group), Student's *t*-test). Thus, DCA significantly alleviated myointima formation. **c**, **d**, In the region of a ruptured internal elastic lamina, the proliferation area (**c**) and the maximal proliferation thickness (**d**) were significantly smaller with DCA (mean ± s.d., $n =$ 42 control sections, $n = 31$ DCA sections, Student's *t*-test). $^{**}P < 0.01$.